Paleolatitudinal Drift and Major Rotation of the Wrangellia Superterrane in the Mesozoic: A Signal of East-Panthalassa Plate Motion?

Goran Andjić[1,2] , **Bram Vaes[1,3]** , **Suzanna H. A. van de Lagemaat[1]** , **Lydian M. Boschman[1]** , **Mark J. Dekkers[1]** , **Stephen T. Johnston[4]** , and **Douwe J. J. van Hinsbergen[1]**

[1]Department of Earth Sciences, Utrecht University, Utrecht, The Netherlands, [2]Institute of Earth Sciences, University of Lausanne, Lausanne, Switzerland, [3]Department of Earth and Environmental Sciences, University of Milano-Bicocca, Milan, Italy, [4]Department of Earth and Atmospheric Sciences, University of Alberta, Edmonton, AB, Canada

Abstract The allochthonous origin of the Wrangellia superterrane relative to North America (NAM) has been established in the early days of plate tectonics using paleomagnetic and geologic data. However, orogenic deformation of the Wrangellia superterrane after its Cretaceous accretion to NAM has complicated the reconstruction of its pre-accretionary tectonic evolution. In particular, vertical-axis rotations linked to strike-slip faulting have cast doubt on the usefulness of paleomagnetic declinations in deciphering its pre-accretionary motions. Here, we compile paleomagnetic data from the Wrangellia superterrane and present new results from uppermost Triassic limestones and lowermost Jurassic lavas of the Bonanza arc, which confirm that it was at those times at a much lower latitude than today (~50°–60°N), at a latitude of either ~25°–30°N or ~25°–30°S. Moreover, declinations reveal a coherent, major clockwise or counterclockwise rotation, depending on hemispheric origin. When correcting for previously documented true polar wander at the approximate longitude of the Wrangellia superterrane at ~190 Ma, new and existing paleomagnetic data allow for two possible scenarios of Mesozoic kinematic evolution: from 190 to 80 Ma, in the southern hemisphere scenario, the Wrangellia superterrane was transported ~5,000 km northward while rotating ~110° clockwise with an associated north-dipping subduction zone, while in the northern hemisphere scenario it remained at northern middle latitudes while rotating ~70° counterclockwise at a south-dipping subduction zone. The southern hemisphere scenario appears more plausible when tested against recent reconstructions of minimum oblique convergence beneath NAM and mantle tomography images of slab remnants.

1. Introduction

The Cordilleran orogen of northwestern North America (NAM) is among the largest accretionary orogens that formed during and since Mesozoic times. The orogen developed at a series of subduction zones that collectively accommodated plate convergence between the major Farallon and several smaller, mostly oceanic Panthalassa plates, and the largely continental NAM Plate (Dickinson, 2004; Engebretson et al., 1985; Nokleberg et al., 2000; Sigloch & Mihalynuk, 2013). Kinematic reconstruction of the Cordilleran orogen of NAM is important for connecting surface geologic processes to mantle dynamics (Sigloch & Mihalynuk, 2017; van der Meer et al., 2010, 2012), exploring economic resources (Nokleberg et al., 2005), and modeling Earth's paleogeography (Scotese, 2021) and paleoclimate (Caruthers et al., 2022; Dal Corso et al., 2020). Restoring the kinematic history of the Cordilleran orogen requires quantifying the amount, timing, and direction of past displacement of the fault-bounded crustal fragments that compose the orogen. This appears at first glance straightforward: the Cordilleran orogen exposes terranes that sutured against the North American margin in the Mesozoic, and that were transported northward since Late Cretaceous times along margin-parallel strike-slip faults, accommodated by complex deformation and oroclinal bending in Alaska (e.g., Cowan et al., 1997; Hildebrand, 2013; Irving et al., 1996; Johnston, 2001). But reading the plate kinematic history that led to the modern orogen has proved challenging.

Orogenic deformation of these terranes has complicated the reconstruction of their pre-accretionary motions. In particular, doubt has been cast on the pertinence of using paleomagnetic data of segments of the North American Cordillera. These data are the most direct quantitative sources to reconstruct past plate motion history, in particular of the rock units that unequivocally underwent a plate motion history within the eastern Panthalassa Ocean, west of NAM, such as the "Wrangellia Superterrane" that is found from British Columbia to Alaska (Figure 1). Well-known problems include: (a) remagnetization of sedimentary and igneous rocks (e.g., Butler,
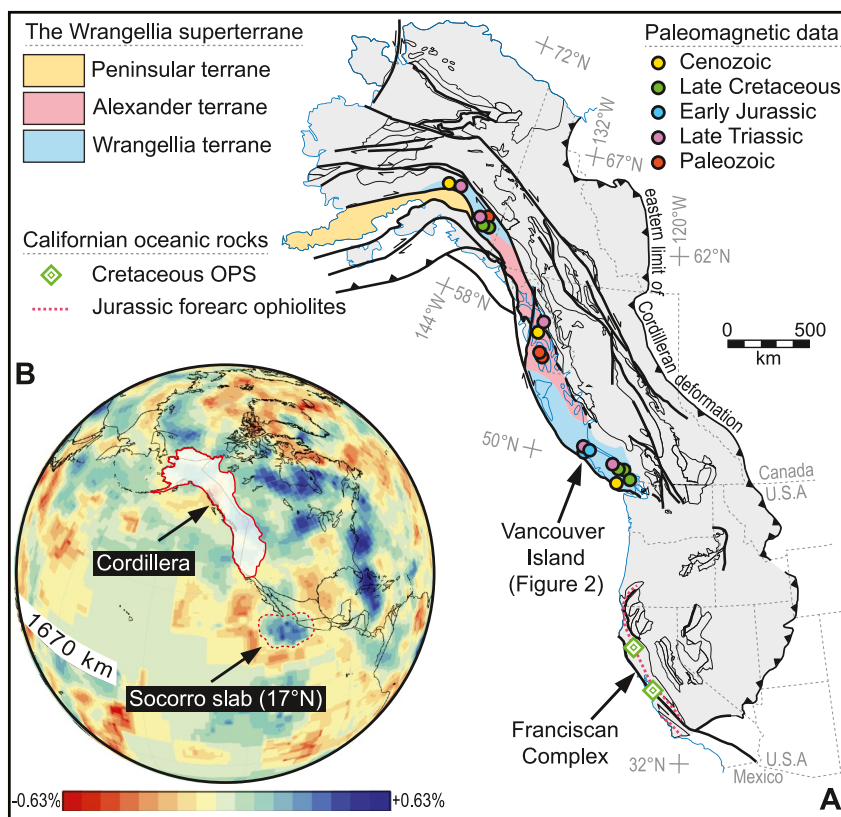
Figure 1. Tectonic setting of the Wrangellia superterrane and other geological records discussed in the text. (a) Tectonic map of the Cordillera of western North America (NAM) (modified after Colpron & Nelson, 2009). The paleomagnetic localities are those of the studies compiled in Figure 7 and in the Data Set S3 (Supporting Information S1). OPS, Ocean plate stratigraphy. (b) UUP07 P-wave tomographic model at 1,670 km depth (Amaru, 2007) showing the location of the Socorro slab (offshore western Mexico) and the outline of the Cordillera of NAM. Positive seismic wave-speed anomalies, such as the Socorro slab, are in blueish colors (up to +0.63%), whereas negative seismic wave-speed anomalies are in reddish colors (down to −0.63%).

Gehrels, & Kodama, 2001); (b) inclination flattening of sedimentary rocks causing underestimation of paleo-latitude (e.g., Krijgsman & Tauxe, 2006); (c) the use of paleomagnetic data obtained from intrusive rocks (e.g., Beck & Noson, 1972; Rusmore et al., 2013), from which interpretation is complicated by a lack of control on paleohorizontal at the time of magnetization; (d) local vertical-axis rotations of blocks during strike-slip faulting making the evaluation of regional (plate) tectonic rotation difficult (e.g., Beck, 1976; Irving et al., 1996). Moreover, recent advances in statistical procedures of paleomagnetic data compilation (e.g., Gallo et al., 2023; Vaes et al., 2023) make it timely to test whether there are flaws in the reference apparent polar wander path (APWP) that quantifies the paleolatitudinal position of NAM (e.g., Kent & Irving, 2010; Torsvik et al., 2012).

In this paper, we re-assess the coherence and consistency of paleomagnetic data from the Wrangellia superterrane. We compiled paleomagnetic data from the Wrangellia superterrane, covering the Paleozoic to Cretaceous, and also compiled data from its post-accretionary Late Cretaceous and Cenozoic rock record. In addition, we collected a new, large paleomagnetic data set from Upper Triassic sedimentary rocks and Lower Jurassic Bonanza arc lavas of the southern Wrangellia superterrane. We use these data to test the reproducibility of existing paleomagnetic data from the youngest Mesozoic age interval for which previous data revealed a subequatorial position. We compare these data to an updated global APWP of Vaes et al. (2023) and evaluate how North American paleomagnetic data sets compare to the global compilation by using data comparison methods (Vaes et al., 2022) that overcome statistical issues of classic paleomagnetic approaches (Rowley, 2019).

In detail, we test whether the paleomagnetic inclinations, estimates of paleolatitudinal position through time, provide a coherent pattern. We also evaluate whether the paleomagnetic declinations, estimating vertical-axis rotations, provide a coherent motion history for the terrane as a whole. We test rates of reconstructed

northward motion of the Wrangellia superterrane against recent reconstructions of minimum oblique subduction components obtained from kinematic evidence from the Californian forearc ophiolites (Arkula et al., 2023) and from Ocean plate stratigraphy (OPS) (rock sequences scraped off subducted ocean floor, including pillow lavas, overlying (hemi)pelagic sedimentary rocks, and foreland basin clastics; Isozaki et al., 1990) accreted in the Californian Franciscan subduction complex (Alvarez et al., 1980; Courtillot et al., 1985; Tarduno et al., 1985, 1986). Finally, we evaluate whether reconstructed positions of the Jurassic Bonanza arc at the time of the end of subduction coincide with the presence of slab remnants in mantle tomography. The updated statistical paleomagnetic procedures and reference frame, as well as the multiple independent tests, will determine whether the extensive rock records of the Wrangellia superterrane dating back to the Paleozoic provide accurate information on the paleolatitudinal and rotational components of its pre-collisional plate motion history relative to NAM.

2. Geological Context

2.1. The Wrangellia Superterrane

Extending from western Alaska to southeastern British Columbia, the Wrangellia superterrane is subdivided into the Peninsular, Wrangellia, and Alexander terranes (Figure 1a), which overall share a multi-stage history of arc magmatism that spans the Late Paleozoic and most of the Mesozoic (~360–100 Ma; Alberts et al., 2021; Nokleberg et al., 1994; Plafker & Berg, 1994). The amalgamation of the three terranes is thought to have occurred during the Paleozoic, prior to their Mesozoic accretion to NAM. East, north, and south of the Wrangellia superterrane are the Intermontane superterrane of the Canadian Cordillera and the Franciscan accretionary prism of Oregon and California, respectively, which both formed as part of the North American margin and consist of metamorphosed continental margin rocks, ophiolites, and accreted complexes that were amalgamated in a subduction zone between the Wrangellia superterrane and the North American continent since the Early Jurassic (Nokleberg et al., 2000; Wakabayashi, 2015). The Wrangellia superterrane is inferred to have been located in an upper plate position relative to a subduction zone that formed the Bonanza arc, but in a downgoing plate position relative to NAM, until its collision with NAM, sometime in the middle to Late Cretaceous (Nokleberg et al., 1994, 2000; Plafker et al., 1989; Tikoff et al., 2023). Such a Mesozoic double subduction system is consistent with slab remains imaged by seismic tomography that revealed parallel belts of mid-mantle slabs below western NAM and the eastern Pacific (Clennett et al., 2020; Fuston & Wu, 2021; Sigloch & Mihalynuk, 2013, 2017; Sigloch et al., 2008; van der Meer et al., 2010, 2012, 2018). Below, we summarize the main geologic features of each terrane and key moments in their tectonic evolution.

The Alexander terrane is interpreted as a microcontinent that was intruded by late Neoproterozoic to early Paleozoic arc-related rocks (~600–400 Ma; Gehrels & Saleeby, 1987; White et al., 2016). Volcanic and plutonic rocks dominate the southern part of the Alexander terrane, whereas its northern part consists mainly of Paleozoic shelf strata as old as the late Cambrian (Beranek et al., 2012). Magmatic activity in the Alexander terrane was interrupted during two orogenic events, the Cambrian Wales orogeny and the Early Devonian Klakas orogeny (Gehrels & Saleeby, 1987).

The Wrangellia terrane consists mainly of Late Devonian to Early Permian and Late Triassic to middle Cretaceous arc-related igneous and sedimentary rocks (Alberts et al., 2021; Nokleberg et al., 1994; Plafker & Berg, 1994). Although basement rocks underlying the Paleozoic arc are not exposed, detrital zircon data from the southern Wrangellia terrane suggest that it incorporated fragments of the Alexander terrane (Alberts et al., 2021). Geologic ties between the Alexander and Wrangellia terranes dating back as early as ~360 Ma (Late Devonian) are corroborated by coeval gabbro complexes that intruded both terranes (Israel et al., 2014).

An episode of plume-related volcanism occurred between the Paleozoic and Mesozoic arc phases of the Wrangellia terrane. The up to 6 km-thick Wrangellia large igneous province (LIP) (Late Triassic, ~232–226 Ma; Greene et al., 2010) is preserved along the full length of the Wrangellia terrane. In our study area on Vancouver Island, the Bonanza arc was built on these flood basalts and associated sedimentary rocks (Canil et al., 2010, 2013; DeBari et al., 1999; D'Souza et al., 2016). The Bonanza Group consists of a basal Upper Triassic–lowermost Jurassic volcanic-sedimentary succession (Parson Bay Formation and Volcaniclastic-Sedimentary unit; ~226–200 Ma, based on detrital zircon U-Pb geochronology and biostratigraphy) overlain by the Lower Jurassic Le Mare Lake Volcanic Unit (~201–190 Ma, based on zircon U-Pb geochronology and biostratigraphy) and the Lower to Middle Jurassic Holberg Volcanic Unit (~201–164 Ma, based on detrital zircon U-Pb and amphibole Ar-Ar geochronology; Nixon & Orr, 2007; Nixon, Hammack, Hamilton, et al., 2011; Nixon,

Hammack, Koyanagi, Payie, et al., 2011; Nixon, Hammack, Koyanagi, Snyder, et al., 2011; Nixon, Snyder, et al., 2011). The younger volcanic units are interbedded with minor marine and non-marine epiclastic rocks and limestone. The bulk of the Bonanza arc complex was intruded by the Early to Middle Jurassic Island Plutonic Suite (~201–164 Ma, based on zircon U-Pb and amphibole Ar-Ar geochronology; D'Souza et al., 2016; Nixon, Hammack, Hamilton, et al., 2011, Nixon, Hammack, Koyanagi, Payie, et al., 2011; Nixon, Hammack, Koyanagi, Snyder, et al., 2011; Nixon, Snyder, et al., 2011). The Le Mare Lake Volcanic Unit and the Island Plutonic Suite represent the main phase of growth of the Bonanza arc. On Vancouver Island, Triassic and younger rocks have experienced zeolite and prehnite-pumpellyite facies metamorphism, implying temperatures below 350°C and pressures below 2.5 kbar (<10 km depth; Kuniyoshi & Liou, 1976; Lei et al., 2020; Morris & Canil, 2022; Stewart & Page, 1974).

Except for the absence of flood basalts, the stratigraphic architecture of the Peninsular terrane is similar to that of the Wrangellia terrane (Figure 1). The Peninsular terrane mainly consists of Late Triassic to Middle Jurassic volcanic, plutonic, and volcaniclastic rocks of the Talkeetna arc, overlain by Upper Jurassic to Lower Cretaceous volcaniclastic basinal strata (McClelland et al., 1992; Plafker et al., 1989; Rioux et al., 2007, 2010). The Talkeetna arc, considered as an archetypal intraoceanic arc, is lithologically, temporally, and geochemically correlative to the Bonanza arc of the Wrangellia terrane (D'Souza et al., 2016; Plafker et al., 1989; Rioux et al., 2007). Scarce outcrops of metamorphosed upper Paleozoic mafic to intermediate volcanic rocks, limestones, and quartz-rich sedimentary rocks provide a glimpse into the basement of the Talkeetna arc (Plafker et al., 1989). Zircon xenocrysts from the Talkeetna arc and younger volcanic products suggest ties with the Alexander and Wrangellia terranes from at least the early Carboniferous (~310 Ma; Amato et al., 2007; Bacon et al., 2012; Beranek et al., 2014).

Based on stratigraphic, structural, geochemical, and geochronologic data from arc and accretionary complex rocks, the polarity of the subduction beneath the Wrangellia superterrane is thought to have been northward in western Alaska and eastward in British Columbia (in present-day coordinates) at least since ~200 Ma (Amato et al., 2013; Clift, Draut, et al., 2005, Clift, Pavlis, et al., 2005; Plafker & Berg, 1994; Trop & Ridgway, 2007). Notably, blueschist-facies metamorphic rocks were formed during the Early Jurassic in a subduction complex now juxtaposed against the outboard (seaward) margin of the superterrane (Roeske et al., 1989; Sisson & Onstott, 1986).

The timing, latitude, and possible diachroneity of the Wrangellia superterrane's accretion to NAM, are not yet resolved. Basinal records in the suture zone between the northern Wrangellia superterrane and the Intermontane superterrane to the east, have been used to suggest timings of collision that include the Middle Jurassic (e.g., McClelland et al., 1992), the Late Jurassic (e.g., Trop & Ridgway, 2007), the Early Cretaceous (e.g., Hampton et al., 2010), the middle Cretaceous (e.g., Amato et al., 2013; Plafker et al., 1989), and the Late Cretaceous (e.g., Hults et al., 2013). Coeval magmatism and development of thrust belts in the Coast Plutonic Complex are inferred to have initiated shortly after collision along the Wrangellia–Intermontane boundary, at ~100 Ma (Journeay & Friedman, 1993; Monger et al., 1982; Rusmore & Woodsworth, 1991). Proponents of diachronous accretion suggest that the southern part of the Wrangellia superterrane in British Columbia collided during the Jurassic, whereas the northern part of the superterrane in Alaska collided during the Late Cretaceous (e.g., Manselle et al., 2020; Trop & Ridgway, 2007). These accretion scenarios mostly differ from each other in the amount of post-subduction translation that the Wrangellia superterrane experienced, based on paleomagnetic studies (Kent & Irving, 2010).

Notably, estimates of post-accretion translation of the Wrangellia superterrane based on detrital zircon data from northern Washington, southern British Columbia, and southern Alaska have not reached any consensus, with offsets ranging from ~500 km (Mahoney et al., 1999, 2021), through ~1,000 km (Yokelson et al., 2015), to >1,500 km (Boivin et al., 2022; Housen & Beck, 1999; Matthews et al., 2017; Sauer et al., 2019). Among these studies, the main disagreement revolves around the source of detrital zircons from the Late Cretaceous Nanaimo Group of Vancouver Island that was deposited on the Wrangellia superterrane, which may have been sourced from rocks outcropping in Idaho (~300–600 km south from Vancouver Island) and/or southern California (~1,500–1,800 km south from Vancouver Island; Boivin et al., 2022, and references therein). In recent models of Late Cretaceous tectonic evolution of the Wrangellia superterrane (e.g., Hildebrand, 2013; Johnston, 2008; Tikoff et al., 2023), both options are compatible with paleomagnetic data from the Late Cretaceous Nanaimo Group,

which have consistently yielded paleolatitudes ∼1,600–2,500 km south of its present-day location (Enkin et al., 2001; Kim & Kodama, 2004; Krijgsman & Tauxe, 2006; Ward et al., 1997).

2.2. Jurassic Ophiolites and Accreted OPS of California

Westernmost California and southern Oregon display a Mesozoic–Cenozoic subduction complex that formed by episodic accretion of OPS, which records the history of a subducting oceanic plate from its formation to arrival at the trench (Isozaki et al., 1990). This subduction complex–the Franciscan Complex–accreted below supra-subduction zone ophiolites of Middle to Upper Jurassic age (∼170–155 Ma) that are preserved as isolated klippen (Wakabayashi, 2015; Figure 1). The oldest accreted rocks are high-temperature, high-pressure meta-basites interpreted as metamorphic sole rocks with Lu/Hf garnet ages of 180 Ma that mark the (minimum) age of subduction initiation (Mulcahy et al., 2018) and show that the ophiolites formed above an active subduction zone (e.g., Guilmette et al., 2018), consistent with their geochemical composition (Snortum & Day, 2020). Using GPlates combined with paleomagnetic data, Arkula et al. (2023) reconstructed western North American deformation to restore the relative positions of the Californian ophiolites in the Jurassic. Their paleomagnetic results also imply that the forearc paleo-ridges that generated the Jurassic ophiolites had near-perpendicular orientations to that of the Franciscan subduction zone. The kinematic restoration of the ophiolite belt shows that the paleo-ridges may have accommodated spreading rates of ∼6 cm/yr, suggesting that the plate subducting obliquely beneath California in the Jurassic had a northward motion relative to NAM of up to ∼6–7 cm/yr.

The Franciscan Complex consists of rocks accreted from oceanic crust that formed since the Early Jurassic (Wakabayashi, 2015). The youngest accretion may have happened as recently as 12 Ma (McLaughlin et al., 1982). Among the accreted rock assemblages, two localities with middle Cretaceous limestone blocks provided paleomagnetic results that allow computing a paleolatitudinal journey of the OPS prior to accretion. The Lay-tonville limestone (103–90 Ma) yielded paleolatitudes of 17° ± 7° (Alvarez et al., 1980) and 14° ± 5° (Tarduno et al., 1986). The Calera limestone (129–90 Ma), located ∼300 km southeast of Laytonville, yielded paleo-latitudes of 24° ± 4° (Courtillot et al., 1985) and 18–25° at 105–90 Ma (Tarduno et al., 1985). Because the blocks may have rotated during accretion to the Franciscan Complex, it is not obvious whether they formed on the southern or northern hemisphere. Also, the accretion age of the limestone blocks to the Franciscan Complex has uncertainties. All scenarios show that in Early to Late Cretaceous times, the OPS sequences that accreted to the Franciscan Complex were derived from lower latitudes, moving north at rates varying from ∼8 cm/yr for the northern hemisphere options (Courtillot et al., 1985; Tarduno et al., 1985) to ≥15 cm/yr for the southern hemisphere options (Alvarez et al., 1980; Tarduno et al., 1986). Additionally, ocean plate igneous and sedimentary rocks with ages ranging from 180 to 110 Ma accreted to the Chortis block around 100 Ma (Andjić et al., 2019) at a latitude of 11°N (Costa Rica): those rocks yielded paleolatitudes of 8–20° north or south (Boschman et al., 2021).

3. Paleomagnetic Sampling and Measurements

To test the robustness of the paleomagnetic data from pre-accretionary rocks of the Wrangellia superterrane, we collected a total of 295 samples for paleomagnetic analysis from four localities in the Bonanza Group of northern Vancouver Island, Canada (Figure 2; Nixon, Hammack, Hamilton, et al., 2011; Nixon, Snyder, et al., 2011). Locality YM ("Yreka Main") was sampled in a continuous ∼50 m monoclinal succession of impure limestones of the Norian–Rhaetian Parson Bay Formation, from which 119 samples were collected (average dip direction = 230°, average dip = 50°, n = 8). Basaltic to andesitic lava flows of the Hettangian–Sinemurian Le Mare Lake Volcanic Unit were sampled in three sections (MD = "Main Drive," TT = "Teeta Creek," VL = "Victoria Lake") that are ∼5 km apart, with each section consisting of ∼15 m (TT: average dip direction = 226°, average dip = 38°, n = 3) to ∼50 m (MD: average dip direction = 273°, average dip = 29°, n = 14; VL: average dip direction = 196°, average dip = 33°, n = 12) of lavas. In our paleomagnetic analysis, we include data from 13 sites sampled by Irving and Yole (1987, abbreviated as I&Y87) along the Cape Perkins locality (average dip direction = 294°, average dip = 52°, n = 4) which is located ∼40 km WNW from our sampling localities.

We used a gasoline-powered motor drill to sample 2.5 cm-diameter paleomagnetic cores, the orientation of which was measured with a magnetic compass with an inclinometer attached. We followed procedures recommended by Gerritsen et al. (2022) and drilled one core per limestone bed or volcanic flow (Figure S1 in Supporting Information S1) to optimize the amount of individual spot readings of the magnetic field, and as a field test selected a
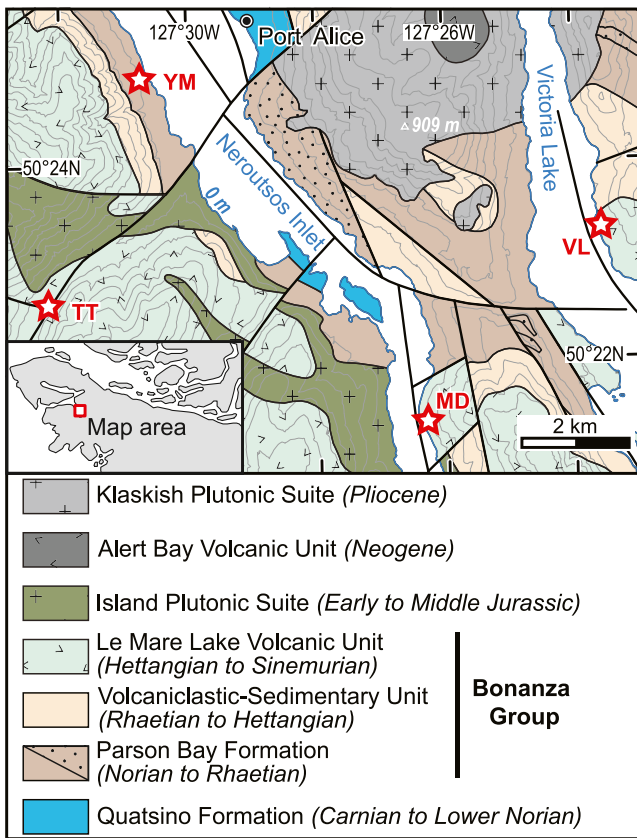
Figure 2. Geological map of the studied area in northern Vancouver Island (100 m contour interval; modified after Nixon, Hammack, Hamilton, et al. (2011); Nixon, Snyder, et al. (2011)), which is shown in the lower left inset. The red stars on the geological map indicate the four localities where paleomagnetic samples were collected. Localities VL, TT, and MD are in the Le Mare Lake Volcanic Unit and locality YM is in the Parson Bay Formation. Parts of the Parson Bay Formation with higher volcaniclastic contents are indicated with a sandy lithological pattern.

total of seven lava sites where 5 cores per lava flow were drilled to evaluate whether within-site scatter of paleomagnetic data is low (i.e., k values typically exceeding 50; e.g., Johnson et al., 2008). Measurements were corrected for the local declination (16°47′E to 16°48′E).

The cores were processed at the Paleomagnetic Laboratory Fort Hoofddijk at Utrecht University, The Netherlands. The cores were cut into 2.2 cm-long samples using a double-blade circular saw. To determine the nature of magnetic carriers for both types of sampled lithology (lavas and impure limestones), thermomagnetic analyses were performed using a horizontal translation-type Curie balance with a sinusoidally cycling applied magnetic field, usually 100–300 mT (Mullender et al., 1993). Several heating-cooling cycles were applied to detect magneto-mineralogical alterations during heating. We used the following temperature scheme (in °C): 150, 75, 225, 150, 300, 225, 375, 300, 450, 375, 525, 450, 600, 20 (for lavas); 250, 150, 350, 250, 450, 350, 520, 420, 620, 500, 700, 20 (for limestones). Stepwise thermal (TH) demagnetization was applied to 117 limestone samples and 30 lava samples, whereas stepwise alternating field (AF) demagnetization was applied to 72 limestone samples and 174 lava samples, the latter processed with a robotized magnetometer (Mullender et al., 2016). Natural remanent magnetizations (NRM) were measured on a 2G DC SQUID magnetometer. Temperature steps of 100, 180, 210, 240, 270, 300, 320, 340, 360, 380, and 400°C were used for TH treatment of 87 limestone samples. Temperature steps of 100, 180, 210, 240, 270, 300, 330, 360, 390, 420, 450, 480, and 510°C were used for TH treatment of 30 other limestone samples. Temperature steps of 100, 180, 210, 240, 270, 300, 330, 360, 390, 420, 450, 480, 510, 540, 570, and 600°C were used for TH treatment of the 30 lava samples. Demagnetization steps of 5, 10, 15, 20, 25, 30, 35, 40, 45, 50, 60, 70, 80, 90, 100, and 120 mT were used for AF treatment of all samples. To improve the resolution of AF demagnetization results of limestones, the latter were heated to 150°C in a thermal demagnetizer prior to AF treatments (van Velzen & Zijderveld, 1995).

Sample interpretation and statistical analysis were conducted using the online portal Paleomagnetism.org (Koymans et al., 2016, 2020). All results can be imported into the portal from data files (.col) available in Data Sets S1 and S2, as well as in the Paleomagnetism.org 2.4.0 database (Koymans et al., 2020). Demagnetization diagrams were plotted on orthogonal vector diagrams (Zijderveld, 1967), and the magnetic components were determined through principal component analysis (Kirschvink, 1980). Remanence directions in orthogonal vector diagrams were determined from at least four successive demagnetization steps, as follows: (a) principal component fits were anchored when demagnetization segments trend clearly toward the origin; (b) principal component fits were not anchored when demagnetization segments do not trend toward the origin. Great circle solutions were determined using the method of McFadden and McElhinny (1988). The fold test (Tauxe & Watson, 1994) and the bootstrap common mean direction test (Heslop et al., 2023) were used when applicable. The elongation-inclination (E/I) method (Pierce et al., 2022; Tauxe & Kent, 2004; Tauxe et al., 2008) was applied to the sedimentary locality. A maximum angular deviation cut off (i.e., MAD ≤15°) was not applied to our data set because it only reduces the number of samples, which decreases paleopole precision (Gerritsen et al., 2022). Paleomagnetic pole positions were calculated using Fisher (1953) statistics on virtual geomagnetic poles (VGPs)–whereby each VGP is derived from a single site–following statistical procedures described in Deenen et al. (2011), providing a measure of the VGP dispersion (Fisher precision parameter, K) and a 95% confidence ellipse on the pole position (A_{95}). The mean paleomagnetic direction and the 95% confidence regions on the declination (ΔD_x) and inclination (ΔI_x) were computed from the paleomagnetic pole and its A_{95}. A 45° cutoff was applied to the VGPs (Johnson et al., 2008) at the group level for the volcanic localities (TT, MD, VL). Application of this cutoff to the sedimentary data set (YM) does not lead to the exclusion of any of the directions.
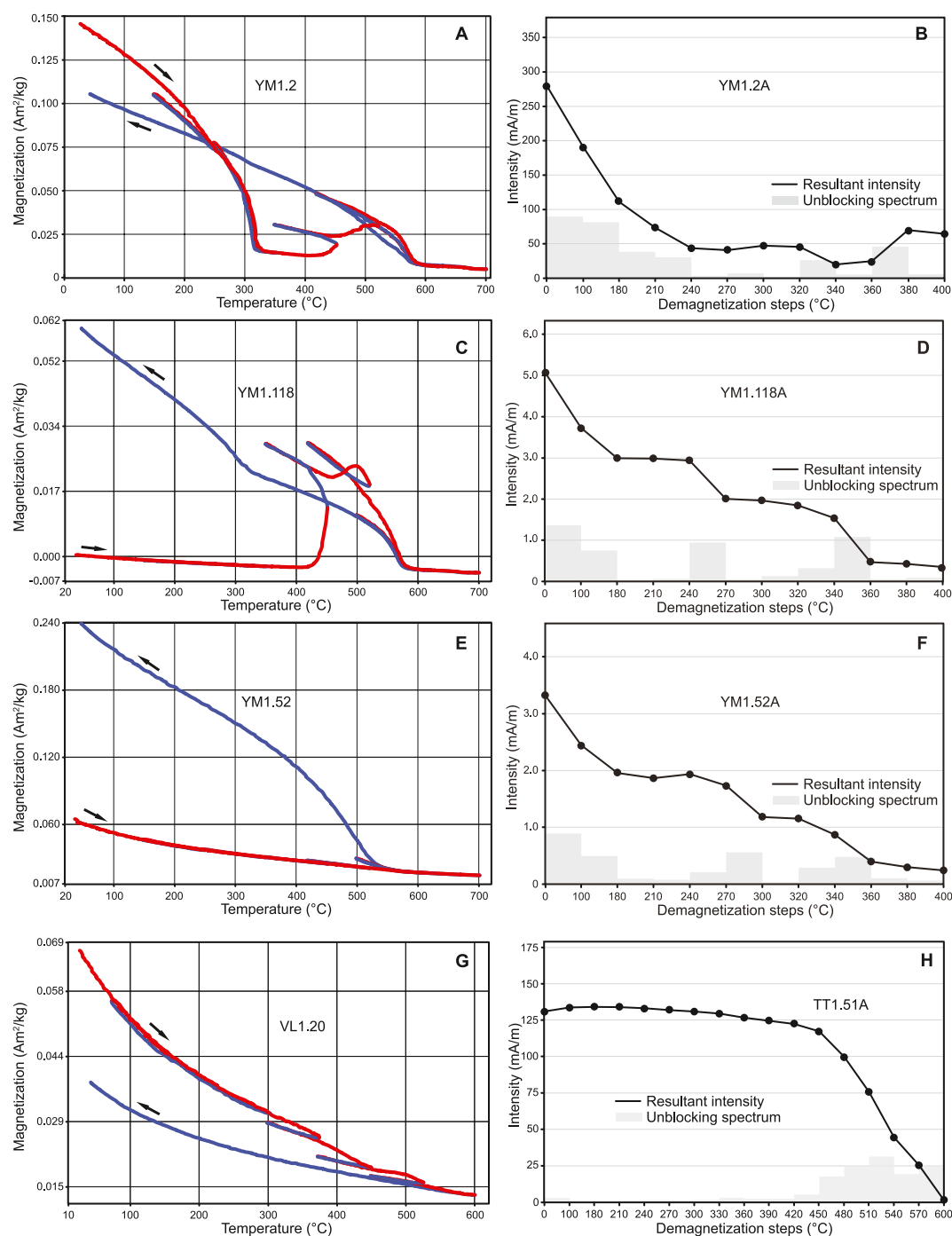
Figure 3. Rock magnetic results from the Parson Bay Formation (YM) and Le Mare Lake Volcanic Unit (TT, MD, and VL). (a), (c), (e), (g) Thermomagnetic curves measured on a Curie balance. Heating segments are in red and cooling segments are in blue. (b), (d), (f), (h) Intensity decay curves measured during thermal demagnetization.

4. Results

4.1. Volcanic Rocks of the Le Mare Volcanic Unit

Thermomagnetic curves show that lava samples have Curie temperatures close to 580°C (Figures 3g and 3h), indicating that magnetite is the main magnetic carrier. In orthogonal vector plots, the majority of the VL (58/80) and MD (32/54) samples reveal an overprint at low temperature/coercivity steps (up to ~100–240°C or 5–15 mT).
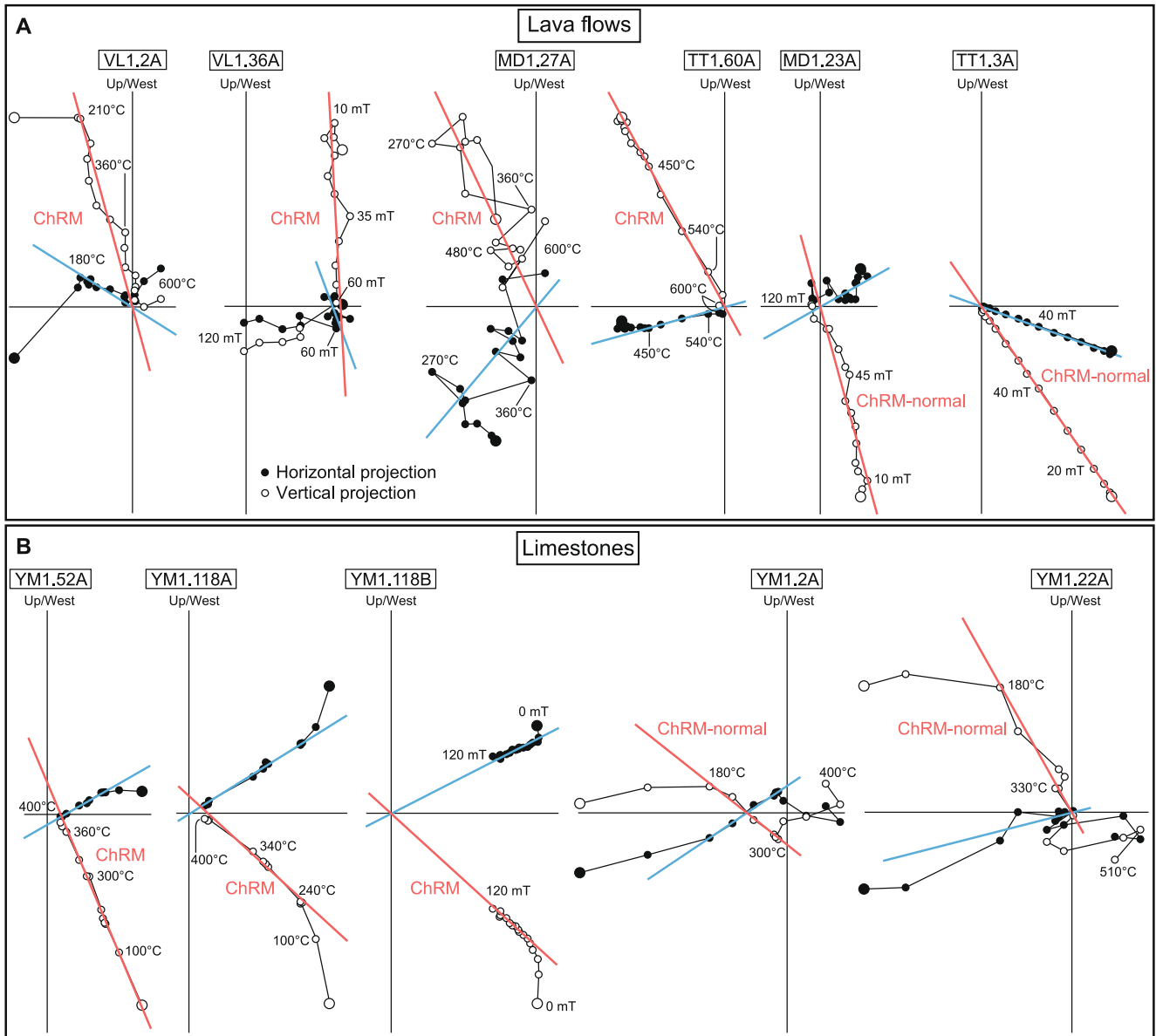
Figure 4. Orthogonal vector diagrams of representative samples from the Parson Bay Formation (YM) and Le Mare Lake Volcanic Unit (TT, MD, and VL) in geographic (= in situ) coordinates, where closed (open) symbols indicate declination (inclination). (a) Six samples from lava flows, including two opposite-polarity directions. (b) Five samples from limestones, including two opposite-polarity directions. ChRM = characteristic remanent magnetization.

VL samples (46/80) have an additional overprint at mid to high-range temperature/coercivity steps (~420–570°C or 15–90 mT), most of which (40/46) did not yield characteristic remanent magnetization (ChRM) directions. In contrast, TT samples show a linear decay toward the origin of demagnetization diagrams without overprints. Initial intensities ranged 7–550 mA/m for TT, 0.2–38 mA/m for MD, and 0.6–1,650 mA/m for VL. ChRM values were generally interpreted between 420 and 570°C or 10–120 mT for TT, ~270–510°C or ~25–70 mT for MD, and ~240–510°C or ~20–70 mT for VL. Interpreted ChRM directions from most samples yielded: (a) southward declinations and steep upward inclinations in in situ coordinates (Figures 4a and 5a); and (b) eastward declinations with shallow upward inclinations in tilt-corrected coordinates (Figure 5b). One TT sample and three MD samples yielded westward, down directions that suggest opposite polarity (Figure 4a); which of these two directions represent normal or reversed is not a priori known, as it depends on the hemisphere of origin. In the MD section, reversed magnetic polarities are located at the level of samples MD 1.23, MD 1.24, and MD 1.40; opposite-polarity ChRM directions of locality MD share a common mean direction.
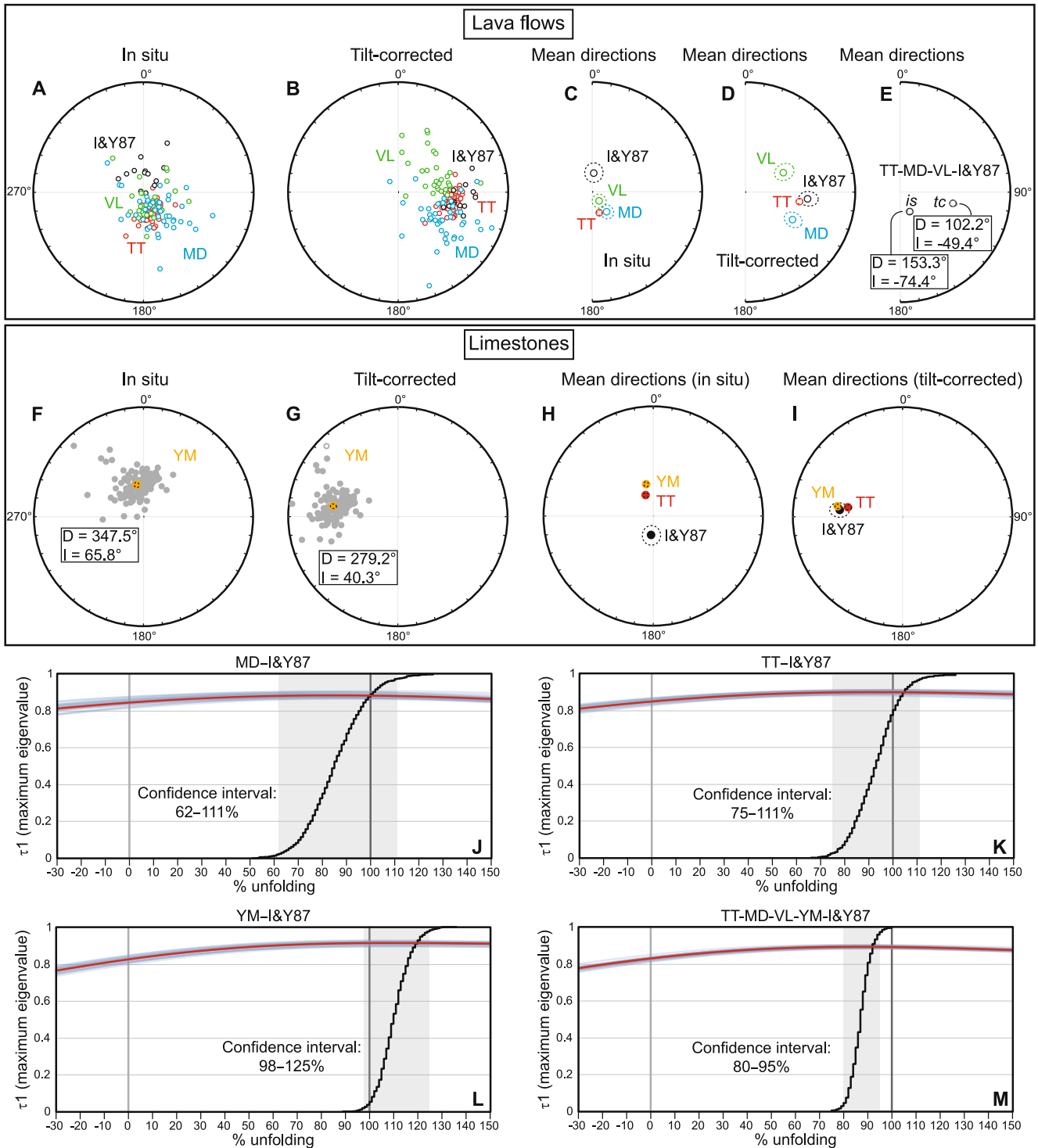
Figure 5. Paleomagnetic results from the Parson Bay Formation (YM) and Le Mare Lake Volcanic Unit (TT, MD, and VL). Data from Irving and Yole (1987) are included. (a), (b), (f), (g) ChRM directions from localities TT (in red), MD (in blue), VL (in green), I&Y87 (in black), and YM (in gray). (a), (f) In situ coordinates. (b), (g) Tilt-corrected coordinates. (c), (d), (h), (i) Mean directions, including confidence intervals (dashed lines), of localities TT, MD, VL, I&Y87 and YM. (e) Mean direction of all volcanic localities, including confidence intervals (dashed lines). is = in situ coordinates, tc = tilt-corrected coordinates. (j)–(m) Bootstrapped fold tests of the sampled localities, with cumulative distribution function (confidence interval in light gray) based on 1,000 bootstrap samples (mean shown in red).

Irving and Yole ([1987](#)) sampled two localities—Cape Perkins and Victoria Lake–in the Le Mare Lake Volcanic Unit of northern Vancouver Island. Their sites 5 and 8 were sampled along the same section as our locality VL. These two sites have northward declination and downward inclination values ($D/I = \sim 025°/\sim 40°$) that are incompatible with the average eastward declination and upward inclination ($D/I = \sim 063°/\sim 58°$) of our data from the same locality. Directions from their sites 5 and 8 are actually comparable to overprints interpreted at mid- to high-range temperature/coercivity steps from the majority of our VL samples (46 out of 80), many of which have very shallow downward inclinations and northward declinations, and did not yield any interpretable ChRM directions (e.g., samples VL1.22–1.25, VL 1.43, VL 1.58–1.70; Data Set [S1](#)). Our sample VL1.36A shows a typical example where both a ChRM and an overprint have been interpreted (Figure [4a](#)). In contrast, 13 sites from Cape Perkins reported by Irving and Yole ([1987](#)) share a common mean direction (in tilt-corrected coordinates) with data from our locality TT (Figure [5i](#)).

Fold tests per section are inconclusive. Differences in bedding orientation among VL, TT, MD, and I&Y87 localities were used in several fold tests, of which the following are considered positive: (a) MD combined with I&Y87 (confidence interval between 62% and 111%, Figure [5j](#)); (b) TT combined with I&Y87 (confidence interval between 75% and 111%, Figure [5k](#)). When the four volcanic localities are combined with the sedimentary locality YM, the fold test yields a result with a confidence interval of 80%–95% (Figure [5m](#)), whereas the combination of the four volcanic localities yields a result with a confidence interval of 64%–85%. We consider that the clustering (<100%) in these regional fold tests may be the result of: (a) uncertainties in bedding tilt correction, which may be primarily related to lava flow emplacement on preexisting topography (e.g., Irving & Yole, [1987](#)); (b) differential block rotations among the lava flow sections. We used the inclination-only method of Arason and Levi ([2010](#)) to compute the mean inclination of the four volcanic localities, which yields a mean ($-50.7° \pm 2.5°$) that is comparable to the Fisher mean presented below ($-49.4° \pm 3.0°$). This implies that local rotations do not have a significant effect on our results from the Le Mare Lake Volcanic Unit.

The lava sites from which we collected multiple samples per site yielded low dispersion (e.g., $k = 395.9$ for TT 1.31–1.35 and $k = 66.9$ for MD 1.16–1.20; Figure S2 in Supporting Information [S1](#)), confirming that lava sites may be treated as spot readings of the field. The paleomagnetic pole computed from the lava sites is located at latitude = 30.8°S, longitude = 339.1°E ($N = 132$, $K = 22$, $A_{95} = 2.7°$), based on a mean paleomagnetic direction of *Declination* (D) $\pm \Delta D_x = 102.2° \pm 3.1°$, *Inclination* ($I$) $\pm \Delta I_x = -49.4° \pm 3.0°$ (Figure [5e](#), Table [1](#)). The D and I values of the combined volcanic localities differ significantly from the recent GAD field (D/I = 000°/70°). The A_{95} value ($A_{95min} = 1.7° < A_{95} = 2.7° < A_{95max} = 3.8°$) satisfies the N-dependent reliability envelope of Deenen et al. ([2011](#)), suggesting that the observed VGP scatter can be explained by paleosecular variation (PSV).

4.2. Sedimentary Rocks of the Parson Bay Formation

Thermomagnetic curves of the limestones are consistent with three types of magnetic carriers. Samples YM 1.91 and YM 1.118 have very low initial magnetization, even diamagnetic susceptibility, that is, the signal is dominated by the quartz glass of the sample holder. The curves are completely reversible after cycling to 250°C and show minor decay after the 350°C cycle, with a pyrite-to-magnetite oxidation signature displayed after 420°C (e.g., Passier et al., [2001](#)). On cooling to room temperature after the 700°C cycle, a discontinuity at ~320°C represents the Curie temperature of pyrrhotite (Figure [3c](#) and Figure S2 in Supporting Information [S1](#)), which is produced during the thermomagnetic experiment. Pyrrhotite is stable with respect to pyrite at high temperatures and apparently not all pyrite is oxidized. If originally present, pyrrhotite would have shown up in the first heating segments as well. In contrast, samples YM 1.52 and YM 1.61 present a much higher (~50–100 times) initial magnetization, with smooth curves that are essentially reversible up to 500°C, which supports the presence of titanomagnetite with a variable Ti content (Figure [3e](#) and Figure S2 in Supporting Information [S1](#)). Interestingly, both groups of samples have similar values of their initial NRM (YM 1.52 = 3.3 mA/m, YM 1.61 = 4.1 mA/m vs. YM 1.91 = 6.0 mA/m, YM 1.118 = 5.1 mA/m), which suggests that the efficiency of the NRM acquisition mechanism differs widely between the two groups. YM 1.91 and YM 1.118 may feature a chemical remanent magnetization, which is an efficient NRM acquisition mechanism. The NRM acquisition of YM 1.52 and YM 1.61 is much less efficient; a lot more magnetic material is required for a similar NRM intensity, which may imply a detrital remanent magnetization. Nonetheless, after thermal demagnetization at 360°C, usually <10%–15% of the initial NRM intensity remains for both types of samples. This result implies that ChRM directions were interpreted from the same temperature steps for both groups. Finally, sample YM 1.2 shows a largely reversible

Table 1
Paleomagnetic Results of the Le Mare Lake Volcanic Unit (MD, VL, TT) and the Parson Bay Formation (YM)

Locality	slat	Slon	N	N45 (is)	N45 (tc)	In situ				Tilt-corrected				k	α_{95}	K	A_{95Min}	A_{95}	A_{95Max}	λ	plat	plong
						D	ΔD_x	I	ΔI_x	D	ΔD_x	I	ΔI_x									
Le Mare Lake Volcanic Unit																						
MD	50.357	−127.439	44	n.a.	n.a.	143.9	15.3	−72.0	5.3	120.3	7.5	−48.9	7.4	15.0	5.8	12.0	2.6	6.5	7.6	−29.8	−43.0	323.6
VL	50.390	−127.392	29	n.a.	n.a.	144.2	37.4	−81.7	5.2	62.6	10.8	−58.2	7.7	18.9	6.3	11.2	3.1	8.4	9.8	−38.8	−16.2	7.3
TT	50.376	−127.546	59	n.a.	n.a.	161.0	6.2	−73.7	1.9	99.9	2.5	−48.6	2.6	98.7	1.9	71.3	2.4	2.2	6.3	−29.6	−28.6	335.6
I&Y87	50.450	−128.050	13	n.a.	n.a.	5.3	28.6	−76.2	7.2	96.1	6.5	−42.2	7.9	49.7	5.9	49.4	4.3	6.0	16.3	−24.4	−22.9	333.7
Mean	50.380	−127.528	145	126	132	153.3	6.4	−74.4	1.9	102.2	3.1	−49.4	3.0	28.8	2.3	22.0	1.7	2.7	3.8	−30.3	−30.8	339.1
Parson Bay Formation																						
YM	50.415	−127.512	139	n.a.	n.a.	347.5	4.1	65.8	2.0	279.2	2.0	40.3	2.5	38.0	2.0	44.7	1.7	1.8	3.7	23.0	23.7	151.3

Note. Data from Irving and Yole (1987) are included. slat/slon = latitude and longitude of sampling location; N = total number of demagnetized samples; $N45$ = number of samples that fall within the 45° cutoff in situ coordinates (is) and after tilt correction (tc); D, ΔD_x = declination and associated error; I, ΔI_x = Inclination and associated error; k and α_{95} = precision parameter and semiangle of the 95% cone of confidence around the computed site mean direction; K and A_{95} = precision parameter and semiangle of the 95% cone of confidence around the mean virtual geomagnetic pole; A_{95max} and A_{95min} = maximum and minimum value of A_{95} expected from paleosecular variation of the geomagnetic field; λ = paleolatitude of the locality; plat/plon = paleopole latitude and longitude; n.a. = not applicable.

thermomagnetic curve with a Curie temperature close to 320°C (Figure 3a), suggesting that an iron sulfide, likely pyrrhotite, is present in the limestone section.

Initial NRM intensities ranged 0.3–400 mA/m, with values mostly restricted to 2–6 mA/m for samples from which ChRMs were interpreted. In orthogonal vector plots, magnetic components could not be determined from a subset of samples (48/189) because of erratic demagnetization behavior. The maximum applicable AF (120 mT) was not high enough to fully demagnetize limestone samples. Nevertheless, ChRM directions interpreted from AF demagnetization data agree well with those obtained from TH demagnetization data, as they share a common mean direction. A few samples (5/140) show an overprint at low temperature/coercivity steps (∼100–210°C or 5–20 mT). ChRM values were generally interpreted at ∼210–360°C or ∼30–70 mT, yielding down, westward directions. Seven YM samples yielded eastward, up directions that suggest opposite polarity; reversed magnetic polarities are located at the base of the section at the level of samples YM 1.1A, YM 1.2A (Figure 4b), YM 1.19A, YM 1.21A, YM 1.22A (Figure 4b), YM 1.22B, and YM 1.23A. Opposite-polarity ChRM directions of locality YM share a common mean direction. The paleomagnetic pole computed for locality YM is located at latitude = 23.7°N, longitude = 151.3°E (N = 139, K = 44.7, A_{95} = 1.8°), providing a direction with $D \pm \Delta D_x = 279.2° \pm 2.0°$, $I \pm \Delta I_x = 40.3° \pm 2.5°$ (Figure 5g, Table 1). The D and I values of YM in tilt-corrected coordinates differ significantly from that of the recent GAD field (D/I = 000°/70°).

Overall, we find that the results of the YM limestones are consistent with dominantly carrying a chemical remanent magnetization. This remanence was acquired soon after sediment deposition and resulted in ChRM acquisition that possibly integrated secular variation over a duration of $\geq 10^3$ yr. This interpretation is compatible with the following aspects: (a) All ChRMs are interpreted between 210 and 360°C and present very high coercivities (no full demagnetization at 120 mT), suggesting that pyrrhotite, a diagenetic mineral, could be the main magnetic carrier of YM samples (e.g., Pastor-Galán et al., 2016). (b) The relatively low dispersion of the VGPs of the limestones yield an A_{95} (1.8°) that is slightly higher than the A_{95min} (1.7°) of the reliability envelope of Deenen et al. (2011); (c) We computed the elongation of the YM data set (in tectonic coordinates) to compare it with the predicted elongation versus inclination curve of the TK03.GAD model of Tauxe and Kent (2004), following the approach of Pierce et al. (2022; Figure S2 in Supporting Information S1). We find that the elongation (∼1.9) predicted by the TK03.GAD curve falls within the bootstrapped 95% confidence range of the YM elongation (1.1–2.6). This indicates that the shape of the directional distribution is consistent with the paleosecular variation model, which is compatible with the acquisition of a chemical remanent magnetization during (early) diagenesis (Pierce et al., 2022). This interpretation is further supported by the fact that YM limestones (age range of about 227 to 201.3 Ma) share a common mean direction with slightly younger lava flows (our TT locality and Cape Perkins of Irving & Yole, 1987, p. 201.3–190.8 Ma; Figure 5i). Moreover, directions of YM limestones and those of Cape Perkins lavas of Irving and Yole (1987) pass a fold test (confidence interval between 98% and 125%; Figure 5l).

Although our preferred interpretation is that of an early diagenetic magnetization, we cannot completely rule out that the YM limestones were remagnetized after the Late Triassic, especially because it was not possible to perform a fold test within the Parson Bay Fm. YM limestones could have been remagnetized at two times: (a) during the Earliest Jurassic, the emplacement of the Bonanza arc could have remagnetized the underlying limestones, which is compatible with the close agreement between YM and TT mean directions; (b) during the Cretaceous–Eocene, remagnetization could have occurred after the tilting of the limestones, which could explain the agreement between the YM mean direction in geographic coordinates and the expected declination (∼340°) and inclination (∼60°) for the sample location for this time period. However, we find the second possibility unlikely, because the geographic mean direction of the YM limestones is comparable to the northward declinations and steep, downward inclinations of the opposite-polarity, geographic mean directions of volcanic sections (TT, VL, and MD).

4.3. Summary of the Results

There is no independent control on the hemispheric origin and direction of rotation (clockwise or counterclockwise) for the YM and combined MD–TT–VL localities, because both normal and reversed magnetic polarities are common in the Norian–Rhaetian and Hettangian–Sinemurian, respectively. Therefore, for each paleomagnetic data set, there are two possible solutions corresponding to either the northern or southern hemisphere, with opposite senses of rotation. The northern hemisphere option for the sediment-derived data set (YM)

yields a paleolatitude of 23.0° ± 2.5° N and a ∼81° counterclockwise rotation (relative to present-day spin axis), whereas the southern hemisphere option yields a paleolatitude of 23.0° ± 2.5° S and a ∼99° clockwise rotation. The combined result of the data from igneous rocks of the Bonanza Group (MD-TT-VL-I&Y87) yields either a northern hemisphere solution with an estimated paleolatitude of 30.3° ± 3.0°N and a ∼78° counterclockwise rotation, or a southern hemisphere solution with a paleolatitude of 30.3° ± 3.0°S and a ∼102° clockwise rotation.

5. Updated Paleomagnetic Data Compilation of the Wrangellia Superterrane

We combine our new data with available paleomagnetic data from the Wrangellia superterrane that we compiled from the literature. We compiled paleomagnetic data from rocks that are located within the boundaries of the Wrangellia superterrane (Figure 1), which includes rocks that were formed before (e.g., Bonanza Group, Karmutsen Formation) and after the accretion of the superterrane (e.g., Nanaimo Group), during the middle Cretaceous. We only chose data from the NW-SE striking part of the Wrangellia superterrane, from southern British Columbia to eastern Alaska. The western and northern parts of Alaska (i.e., Peninsular terrane) were not included in the compilation, as these were proposed to have been rotated in Late Cretaceous to Paleocene times during oroclinal bending (Box, 1985; Dover, 1994; Johnston, 2001). Our data compilation includes data sets that contain at least eight individual directions of the magnetic field (either from eight individual cooling units in magmatic rocks, or eight sedimentary beds, as suggested by Meert et al., 2020), and of which the distribution of VGPs passes the Deenen et al. (2011) criterium of representing paleosecular variation ($A_{95min} < A_{95} < A_{95max}$). We included sediment-derived data sets that were not corrected for potential inclination shallowing and thus do not satisfy the recently proposed reliability criteria for sedimentary data sets of Vaes et al. (2021). We do so to increase the temporal coverage of our data compilation, including, for instance, the data sets derived from Paleozoic (Bazard et al., 1995; Van der Voo et al., 1980) and Upper Cretaceous sedimentary rocks. We excluded data sets from the compilation if the authors of the original study interpreted the magnetic signal to represent a remagnetization (Butler et al., 1997; Haeussler, Coe, & Onstott, 1992; Hillhouse & Grommé, 1980; Irving & Massey, 1990; Symons, 1985), rocks with an unknown paleohorizontal were sampled (Irving et al., 1985; Irving & Massey, 1990; Rusmore et al., 2013; Symons, 1973), or shearing was interpreted to have influenced the magnetic directions (Butler et al., 2002).

Our compilation contains data sets for Early Jurassic and older times, and for Late Cretaceous and younger times. There are two small data sets from Lower Cretaceous strata in Alaska that were collected by Stone et al. (1982), and some preliminary results provided by Panuska et al. (1984). However, the original data and descriptions are not available, and the data sets were considered unreliable in subsequent studies (Butler et al., 1997; Harbert, 1990; Hillhouse, 1987). In addition, we excluded the paleomagnetic results from the mid-Cretaceous (∼110 Ma) ultramafic rocks of Duke Island (Bogue & Grommé, 2004) due to the low number of sites ($N = 6$) and the uncertainties surrounding the determination of the paleohorizontal (Bogue & Grommé, 2004; Butler, Gehrels, & Saleeby, 2001). Butler et al. (1997) revisited Ordovician, Silurian, Devonian, and Carboniferous rocks of the Wrangellia superterrane from which Van der Voo et al. (1980) reported paleolatitudes. Butler et al. (1997) argued that the magnetizations carried by these Paleozoic rocks are largely secondary, concluding that none of these provide useful paleogeographic information. We show the data of Van der Voo et al. (1980) in our compilation but we consider them as potentially unreliable, as discussed further in Section 6.1.

The final compilation consists of a total of 38 collections from 17 studies, 23 for the Late Cretaceous and younger, and 15 for pre-Late Cretaceous times (Tables S1 and S2 in Data Set S3). For Late Cretaceous and younger times, paleolatitudes are all ∼30° or higher and interpreted as northern hemispheric. For the older data sets, paleolatitudes can be either southern or northern hemispheric. The exception are rocks from the Late Carboniferous-Permian Kiaman superchron (∼320–260 Ma; Opdyke & Channell, 1996), which must be of reversed polarity if they carry a primary magnetization (Panuska and Stone, 1981). In Section 6.2, we show and discuss both hemispheric options.

6. Discussion

6.1. Paleomagnetic Data From the Wrangellia Superterrane: Paleogeographic Drift or Artifact?

To evaluate the paleomagnetically permissible plate motions of the Wrangellia superterrane since the Triassic, we use the updated paleomagnetic data compilation that includes our two new paleomagnetic poles. First, we briefly re-evaluate whether the new global APWP of Vaes et al. (2023) for the last 320 Ma provides significant
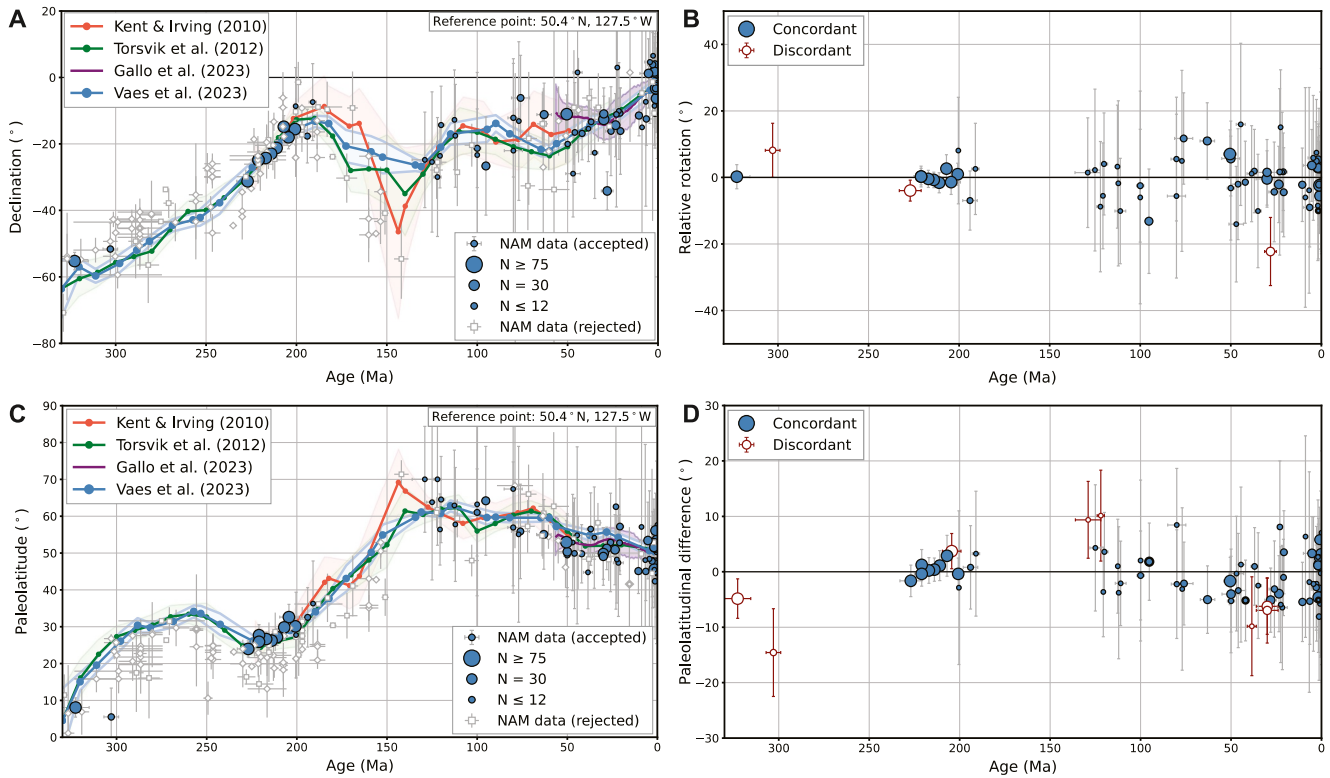
Figure 6. Declination (a) and paleolatitude (c) curves for the North American plate at a reference point at 50.4°N and 127.5°W, as predicted by three global APWPs and the high-resolution apparent polar wander path (APWP) for NAM by Gallo et al. (2023). The colored bands show the 95% confidence regions for each curve. Note that the global APWP of Kent and Irving (2010) and the APWP of Gallo et al. (2023) do not cover the entire time range discussed here. Markers show declination and paleolatitude values computed from paleomagnetic data sets from stable NAM (compiled by Vaes et al., 2023), with error bars that indicate the age uncertainty and 95% confidence in the declination or paleolatitude. Blue dots and white squares/diamonds indicate data sets that were accepted or rejected for inclusion in the global APWP of Vaes et al. (2023), respectively. The diamonds represent sediment-derived data sets that were not corrected for inclination shallowing, whereas the squares indicate data sets from igneous rocks. Relative rotations (b) and paleolatitudinal differences (d) between the accepted North American data and the global APWP are computed using the data-comparison approach of Vaes et al. (2022), in which the uncertainties of the reference poles provided by the APWP are weighted against the number of sites that underlie the investigated data sets. Discordant (i.e., statistically different from zero) results are colored in white with red edges and error bars.

modifications to the paleolatitude and declination reference curves for the North American continent that would alter the previous interpretations of Wrangellia-North America motion. This new APWP is based on (re-sampled) site-level paleomagnetic data rather than on study-mean paleomagnetic poles, which were previously used for APWP computation (e.g., Kent & Irving, 2010; Torsvik et al., 2012; see Vaes et al., 2022, 2023, for details). First, as illustrated in Figure 6, the global APWP of Vaes et al. (2023) gives a smaller uncertainty but is mostly within error of widely used global APWPs (in North American coordinates) of Kent and Irving (2010) and Torsvik et al. (2012). Second, we evaluate whether paleomagnetic data sets from stable NAM that contributed to the global APWP are anomalous. Therefore, we have plotted all data derived from NAM that were used in the construction of the global APWP of Vaes et al. (2023; Figure 6), as well as the North American data that were included in previous global compilations but did not satisfy the selection criteria used by Vaes et al. (2023). Most of the accepted North American data are in excellent agreement with the declination and paleolatitude predicted by the global APWP, including the Late Triassic and Early Jurassic data. When comparing these data directly with the predicted values of the global APWP using the data-comparison approach of Vaes et al. (2022), we find that only 3 out of 74 data sets (~4%) have a statistically different declination, and 8 out of 74 data sets (~11%) have a significantly different paleolatitude. These results are consistent with those obtained earlier by Enkin (2006), who found similar agreement between global and North American data. Third, we show the predicted declination and paleolatitude curves based on the 1-Ma-resolution North American APWP for the last 56 Ma of Gallo et al. (2023). These curves are again statistically indistinguishable from those of the global APWP of Vaes et al. (2023), although the curve of Gallo et al. (2023) predicts a paleolatitude that is ~3° lower between about 30

and 56 Ma. Based on these observations, we regard the global APWP of Vaes et al. (2023) as a reliable reference curve against which the data from the Wrangellia superterrane can be compared.

Most previous studies assessed tectonic motions of mobile terranes such as the Wrangellia superterrane relative to NAM by using pole-to-pole comparisons between poles obtained from a mobile terrane and individual study-mean poles of "cratonic" NAM (e.g., Dickinson & Butler, 1998; Irving & Wynne, 1990; Tikoff et al., 2023). However, the dispersion of reliable paleomagnetic reference poles from stable NAM (Figure 6) indicates that such an approach may be less robust compared to using a global APWP as a reference, which is based on considerably more data and has a significantly more robust temporal coverage (e.g., Enkin, 2006). This scatter among coeval paleomagnetic poles from stable parts of continents was previously observed by Harrison and Lindh (1982) and, more recently, Rowley (2019) and Vaes et al. (2022), and has been shown to be mostly caused by the under-sampling of paleosecular variation of the past magnetic field. A considerable portion of the North American data that do not pass the selection criteria of Vaes et al. (2023) have been included in previous compilations of North American reference poles as well as for the computation of reference APWPs. The use of these poles may have influenced previous calculations of tectonic displacements of Cordilleran terranes relatively to the North American plate, particularly for Jurassic and older times. In addition, we note that different data selection criteria have led to substantially different Jurassic APWPs for NAM. For instance, the inclusion or exclusion of Jurassic paleomagnetic poles derived from Adria (rotated to North American coordinates; Muttoni & Kent, 2019) or from the Middle Jurassic Summerville and Morrison Formations (Mirzaei et al., 2021) have strong influence on the resulting APWP. We emphasize that the choice of a reference APWP will influence plate tectonic reconstructions of NAM and exotic terranes such as the Wrangellia superterrane.

Here, we compare the data of the Wrangellia superterrane with the global APWP in North American coordinates of Vaes et al. (2023) for the last 320 Ma, and with the running mean, 'pole-based' APWP for Laurentia of Torsvik et al. (2012) for earlier parts of the Paleozoic (Figure 7). Plotting the data compilation against a North American reference curve for both northern (N) and southern (S) hemisphere scenarios allows us to re-evaluate previous hypotheses on the primary or secondary nature of specific paleomagnetic data. First, both declinations and inclinations from Paleozoic to Early Jurassic rocks of the Wrangellia superterrane are systematically different from those of the Late Cretaceous to Cenozoic rocks. If a regional unrecognized remagnetization in Late Cretaceous or younger times had occurred, creating apparently low paleolatitudes by erroneously correcting for bedding tilt (Butler, Gehrels, & Kodama, 2001; Hollister et al., 2004; Housen & Beck, 1999; Monger & Price, 1996; Nelson & Colpron, 2007), then that remagnetization process would also have likely affected older rocks. The coherent, systematically deviating paleomagnetic directions of pre-Late Cretaceous rocks make a regional remagnetization in Late Cretaceous or younger times unlikely. Rather, remagnetization processes during those times are considered to be localized (e.g., Housen, 2018).

On the other hand, previous arguments for remagnetization of Paleozoic rocks (Butler et al., 1997) cannot be excluded. Rocks older than the Triassic have declinations as well as inclinations that are similar to those from the Triassic Wrangellia LIP (Figure 7). If they were not remagnetized during the eruption of the LIP, these rocks would suggest that for a period of ~250 Ma, from the Devonian to the Triassic, Wrangellia was part of a plate that was not moving much in paleolatitude, nor undergoing systematic vertical-axis rotations. We therefore avoid interpreting the pre-Triassic history of Wrangellia here in detail. However, the northern hemisphere-counterclockwise rotation scenario permits interpretation of the available Paleozoic data as primary. In contrast, the southern hemisphere-clockwise rotation scenario requires that at least the rocks from the Carboniferous-Permian Kiaman superchron do not carry a primary magnetization. Future detailed paleomagnetic study of these rocks may resolve this difference.

6.2. Paleomagnetic Constraints on Wrangellia Plate Motion Since the Triassic

When taking the APWP of NAM as a reference, the paleomagnetic data set of the Wrangellia superterrane yields two hemispheric options with consistent declinations (Figure 7). These clusters imply either ~100° clockwise or ~80° counterclockwise rotation relative to the magnetic north pole since the Early Jurassic. Previous workers have mostly focused on paleolatitudes and assumed that declinations were unreliable to constrain the pre-accretionary rotation of the Wrangellia superterrane because of local rotations related to post-accretionary orogenic deformation (e.g., Beck, 1976; Kent & Irving, 2010). Such local rotations could be explained, given that the Cordilleran orogen has been folded, faulted, and transported northward along the North American margin,
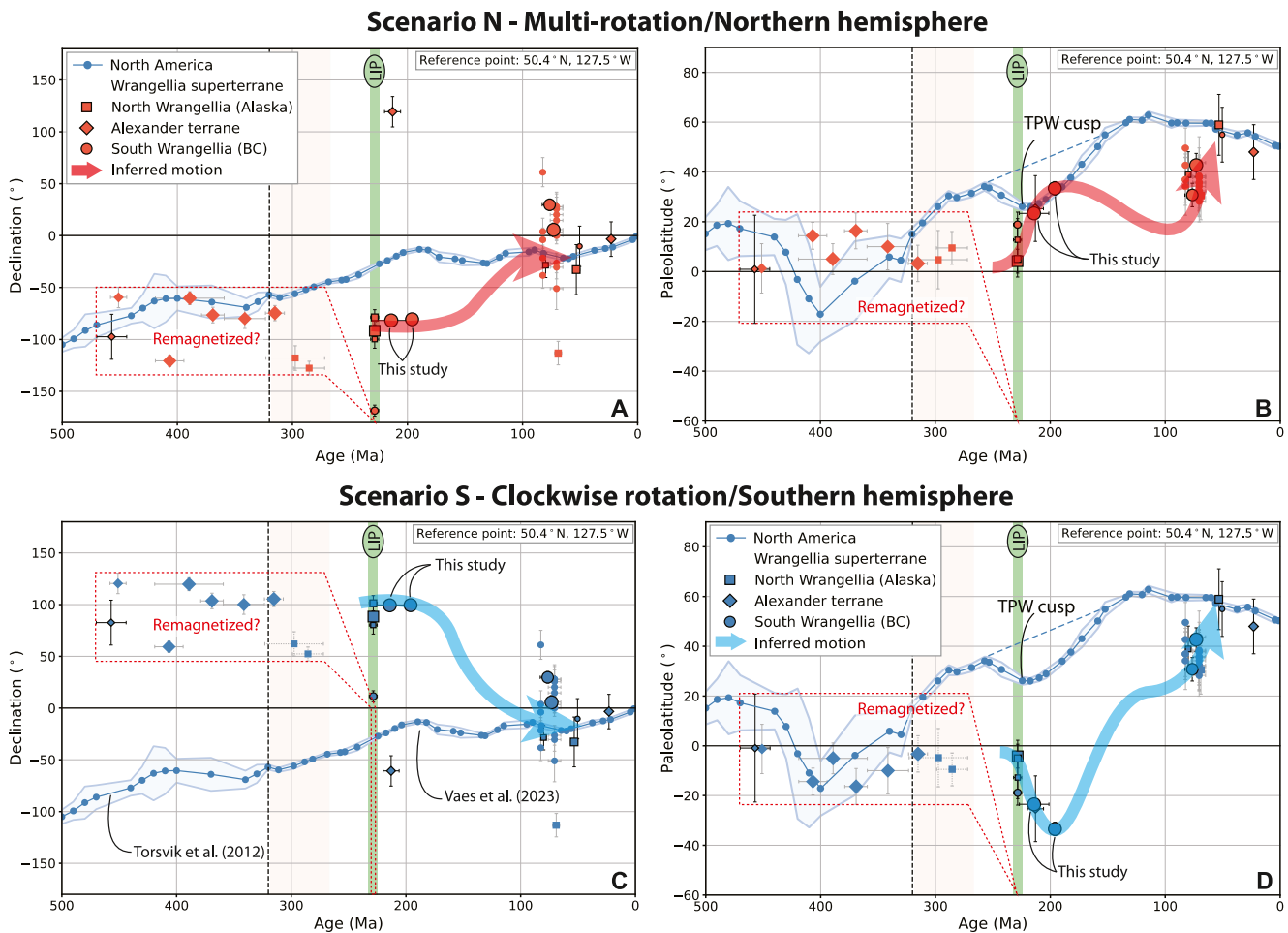
Figure 7. Paleomagnetic results obtained from the Wrangellia superterrane compared to predicted values for North America (NAM). Two possible scenarios are permitted by the hemispheric ambiguity of the pre-100 Ma paleomagnetic data: the upper panels (a, b) show Scenario N (northern hemisphere) and the lower panels (c, d) show Scenario S (southern hemisphere). Declination and paleolatitude values are computed for a reference point at 50.4°N and 127.5°W and are shown as blue or red dots with error bars indicating the age uncertainty and 95% confidence in the declination or paleolatitude. The marker symbol shows from which part of the Wrangellia superterrane the data was obtained. Symbols with black edges and error bars indicate data sets from igneous rocks or sediment-derived data sets that were corrected for inclination shallowing. Predicted declination and paleolatitude curves–based on the global apparent polar wander path (APWP) of Vaes et al. (2023) for the last 320 Ma and North American APWP of Torsvik et al. (2012) for 320–500 Ma (transition marked by vertical dashed line)–are shown as blue curves (with 95% confidence region). The Carboniferous-Permian Kiaman superchron (~320–260 Ma) is indicated by the colored band. The expected reversed polarity for the data from the superchron requires those plotted for Scenario S to be remagnetized (indicated by dashed error bars). The inferred effect of Triassic-Jurassic TPW on the paleolatitude of NAM is highlighted. Paleomagnetic data are derived from the following sources (for numerical values, see Table 1 and Tables S1 and S2 in Data Set S3): Hillhouse (1977), Van der Voo et al. (1980), Yole and Irving (1980), Panuska and Stone (1981), Hillhouse and Grommé (1984), Panuska (1985), Hillhouse et al. (1985), Irving and Brandon (1990), Haeussler, Coe, and Onstott (1992), Haeussler, Coe, and Renne (1992), Bazard et al. (1995), Ward et al. (1997; E/I correction fromKrijgsman and Tauxe (2006)), Enkin et al. (2001), Stamatakos et al. (2001), Kim and Kodama (2004; E/I correction from Krijgsman and Tauxe (2006)), and this study. LIP, Large Igneous Province.

possibly along major strike-slip faults (Beck, 1976, 1980; Irving & Yole, 1987). However, inspection of the data compilation does not suggest that local rotations play a major role. The scatter in declinations for collections of Late Cretaceous rocks of the Wrangellia superterrane is several tens of degrees. Much of these data collections are small, based on a dozen or so paleomagnetic sites (Tables S1 and S2 in Data Set S3). As mentioned above, even the declinations obtained from data sets of the stable plate interior of NAM (and provided input for global APWPs) are scattered over 30–40° (Figure 6a). This large dispersion of coeval paleomagnetic poles was previously shown to predominantly result from limited averaging of paleosecular variation (Harrison & Lindh, 1982; Vaes et al., 2022). The declination scatter of data from the Wrangellia superterrane is larger than that, suggesting that local tectonic rotations enhanced it. Nonetheless, the declinations of Triassic and Jurassic rocks are not chaotic: Lower Mesozoic and older rocks yield declinations that are systematically much larger than those of the

Upper Cretaceous rocks, but their scatter is similar to the latter. Similarly, the declination scatter of Paleozoic rocks from the Alexander and northern Wrangellia terranes is large but not chaotic. Importantly, declinations of Paleozoic rocks are strongly rotated and overlap those of Late Triassic rocks. We consider that these paleomagnetic data are not suitable to infer the paleogeographic evolution of the Alexander and northern Wrangellia terranes throughout the Paleozoic because they could have been the result of remagnetization during the Late Triassic. However, paleomagnetic data from Paleozoic rocks taken together with paleomagnetic data from Late Triassic–Early Jurassic rocks support the view that large magnitude rotations are the result of pre-accretionary plate motions of the Wrangellia superterrane, rather than the consequence of post-accretionary vertical-axis rotations linked to orogenic deformation. We therefore infer that the Wrangellia superterrane underwent a coherent rotation between the Early Jurassic and the Late Cretaceous, that is, during the pre-collisional period when it was part of a plate converging with NAM (Tikoff et al., 2023). In a southern hemisphere scenario (Scenario S), this corresponds to a ~110° clockwise rotation relative to NAM, whereas in a northern hemisphere scenario (Scenario N) it represents a counterclockwise rotation of ~70° (Figure 7).

Previous data from Triassic and older rocks of the Wrangellia superterrane yield paleolatitudes close to the equator (Figure 7). Our new data set shows a rapid paleolatitudinal motion on the order of 20–30° in the Late Triassic to Earliest Jurassic, which is northward in Scenario N, and southward in Scenario S (Figure 7). In Scenario S, this is followed by a northward motion of ~50° in ~110 Ma (~5 cm/yr). In Scenario N, paleolatitudes would remain fairly constant until the Late Cretaceous.

To interpret what such paleolatitudinal changes would mean for plate motion rates, we compare these trajectories with the paleolatitudinal motion of cratonic NAM. Scenario S gives a southward shift of the Wrangellia superterrane in the Triassic, followed by a northward motion (Figure 7). Interestingly, a southward trajectory is also visible from Late Triassic to Early Jurassic time in the global APWP in North American coordinates, superimposed on a northward trend. This 'dip' is observed worldwide and is interpreted as a major phase of True Polar Wander (TPW) that occurred in Late Triassic to Jurassic times (Steinberger & Torsvik, 2008; Torsvik et al., 2012; Vaes & van Hinsbergen, 2024). TPW is the tilting of the solid Earth relative to the spin axis, which results from changes in its moment of inertia, mostly because of the slow sinking of slabs through the mantle (Steinberger & Torsvik, 2010) and is directly detected as the difference between plate motions in a paleomagnetic reference frame (which includes TPW effects), and a mantle reference frame (which is blind to TPW effects; e.g., van Hinsbergen et al., 2015). It is important to realize for comparing Wrangellia's paleomagnetic data with a North American reference curve that the magnitude of TPW-induced paleolatitudinal change is paleolongitude-dependent. Comparison between the paleomagnetic reference frame of Vaes et al. (2023) with the recent mantle reference frame of Müller et al. (2022) suggested that the pole of TPW was located at the equator (by definition), within the Atlantic Ocean (Vaes & van Hinsbergen, 2024), consistent with earlier estimates (Steinberger & Torsvik, 2008). At the longitude of western NAM, this TPW phase caused a southward and then northward shift in latitude on the order of 15° with a peak magnitude of TPW around 200 Ma. Farther west, in the eastern Panthalassa Ocean where the Wrangellia superterrane must have been, the magnitude of TPW increased up to a maximum of ~20°. Much of the southward shift from the equator to >20°S in Scenario S could thus result from TPW rather than plate motion relative to the mantle. Because Jurassic motion of NAM was northward, northward motion of the Wrangellia superterrane relative to NAM was ~50° between ~190 and ~80 Ma, a period of 110 Ma in Scenario S, that is, an average northward relative plate motion rate of ~5 cm/yr superimposed on a paleomagnetically unresolved eastward, convergent motion component (Figure 7). There are currently no high-quality paleomagnetic data to further specify how this relative northward motion was distributed through time.

Scenario N requires a rapid northward shift of ~30° of the Wrangellia superterrane in the Late Triassic to Earliest Jurassic. It is important to note that this motion is opposite to the TPW-induced southward motion, which means that the plate tectonic motion in Scenario N is larger, by about ~20°, than the paleomagnetically determined motion. This would result in a relative northward plate motion component of Wrangellia of ~50° between 220 and 190 Ma, that is, almost 20 cm/yr, and requires that it was followed by a net paleolatitudinal standstill of the plate carrying the Wrangellia superterrane until the Late Cretaceous. Because NAM continued moving northwards in the Jurassic, the plate carrying the Wrangellia superterrane would have to have moved southwards relative to NAM at a few cm/yr, that is, with a left-lateral strike-slip component. Below, we place both scenarios in further plate tectonic context.
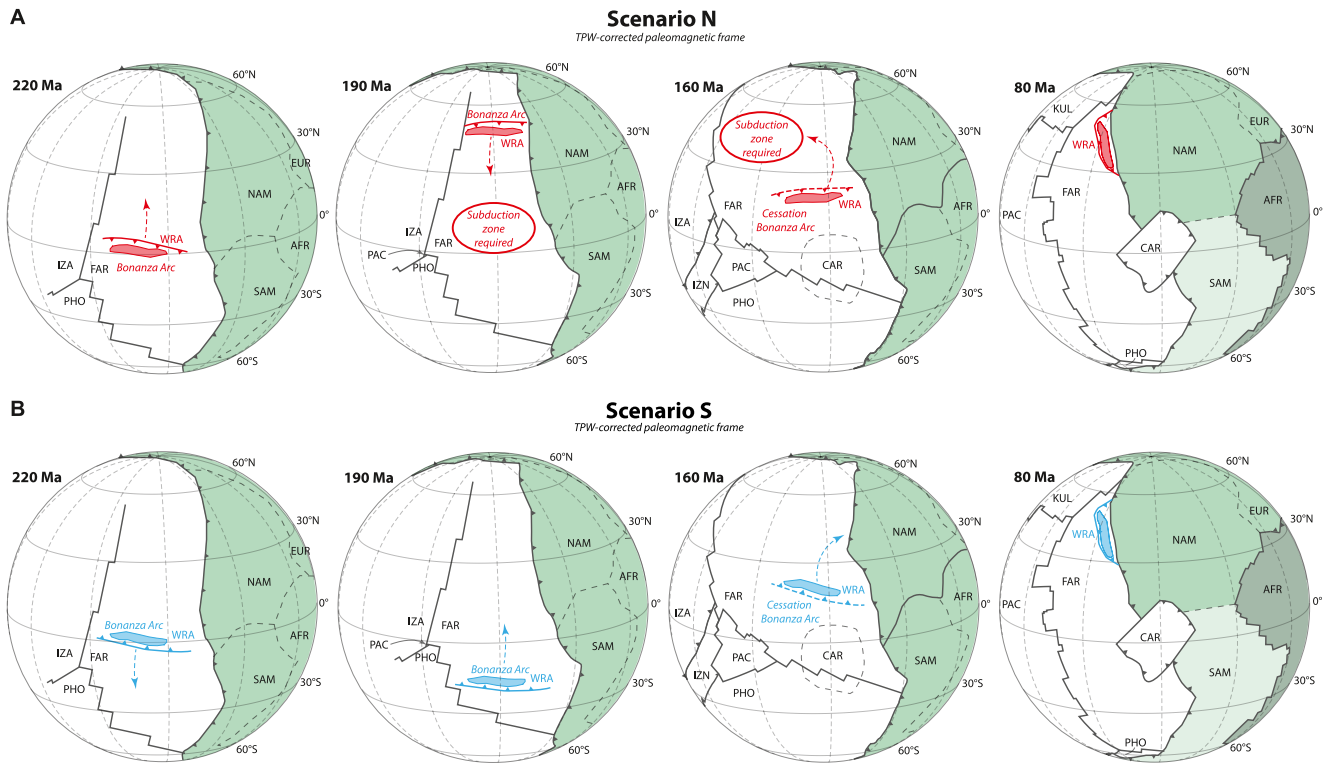
Figure 8. Schematic kinematic scenarios of the motion of the Wrangellia superterrane during the Late Triassic to Late Cretaceous (220–80 Ma). (a) Scenario N depicts a rapid Late Triassic–Early Jurassic northward shift of ~50° in the northern hemisphere, followed by a southward motion of lower amplitude, and then a standstill at middle latitude accompanied by counterclockwise rotation of ~70°. (b) Scenario S shows a Late Triassic–Early Jurassic southward motion of ~15° followed by a northward motion of ~5,000 km from the southern hemisphere accompanied by a clockwise rotation of ~110°. AFR, Africa; CAR, Caribbean; EUR, Europe; FAR, Farallon; IZA, Izanagi; IZG, Izanami; KUL, Kula; NAM, North America; PAC, Pacific; PHO, Phoenix; SAM, South America; WRA, Wrangellia.

6.3. Wrangellia in Context of Eastern Panthalassa Plate Kinematic History

We explore the plate tectonic consequences and feasibility of the paleomagnetic scenarios above. A detailed kinematic restoration of Cordilleran orogenic architecture is required to fully justify a final choice between the two options. Such a reconstruction is beyond the scope of the current paper. We therefore restrict ourselves here to outlining the implications, solutions, and problems that the two scenarios generate.

We present a simplified tectonic reconstruction in Figure 8. We assume a 190 Ma-position of ~30° south or north of a simple, straight Wrangellia superterrane–which does not include the parts bent into Alaska (Johnston, 2001)– relative to NAM in the paleomagnetic reference frame of Vaes et al. (2023). Because we aim to develop a plate tectonic scenario and compare it to seismic tomographic constraints, we place the reconstruction in the TPW-corrected paleomagnetic reference frame of Torsvik et al. (2012). The latter frame has no paleolongitudinal constraints, so we restrict ourselves in the comparison to tomography and latitudinal fits only.

The paleolongitudinal position of the Wrangellia superterrane relative to the Americas is not constrained by paleomagnetism, but options are restricted given the estimated position of the Farallon-Phoenix-Izanagi triple junction at which the Pacific Plate formed at 190 Ma (Boschman & van Hinsbergen, 2016). The position of this triple junction must have been located in the eastern Panthalassa Ocean to maintain convergence of the major Panthalassa plates with the surrounding continents, and we use the approximated position of Boschman et al. (2021). This reconstruction gives the Wrangellia superterrane a possible paleolongitudinal range of ~5,000 km at 190 Ma.

From Late Triassic (~210 Ma) to Middle Jurassic times (~165 Ma), when the Bonanza arc was active, the Wrangellia superterrane was in an upper plate position of a subduction zone. In present-day coordinates, the trench is thought to have been located to the west of the Wrangellia superterrane (Clift, Pavlis, et al., 2005; Trop & Ridgway, 2007). This geometry requires that in Scenario S, the Wrangellia superterrane was underlain by a

northward dipping subduction zone. In Scenario N, the Wrangellia superterrane was underlain by a southward dipping subduction zone.

We evaluate the scenarios against the evidence for oblique subduction below the California forearc between 170 and 160 Ma with a N-S component of ∼6–7 cm/yr, deduced from reconstructing the Californian ophiolites (Arkula et al., 2023), and the evidence for a northward motion component throughout the Cretaceous as suggested by the paleolatitudes of the accreted seamounts of the Franciscan accretionary complex of California (Courtillot et al., 1985; Tarduno et al., 1985, 1986). In addition, a northward motion component is also permitted that is in line with the OPS that accreted to the western margin of the Chortis block in the Early Cretaceous, although a stable eastward relative plate motion is also permitted there (Boschman et al., 2021).

We use two additional constraints in the 190–80 Ma time window to illustrate the implications of the two scenarios. First, the Caribbean Plate contains Jurassic crust that formed around ∼160–150 Ma, and that was part of the Farallon Plate prior to the ∼100 Ma onset of subduction at the western Caribbean subduction zone (Boschman et al., 2019). This crust likely formed at the Farallon-Phoenix spreading ridge, and paleomagnetic data reveal that this crust was located near the equator during the Late Jurassic (Boschman et al., 2019). This requires that, by ∼160 Ma, the Wrangellia superterrane must have been located to the north of the Caribbean lithosphere, and that it has likely always been located to the north of the Phoenix-Farallon spreading ridge.

Second, the Bonanza arc must have been associated with a subducting slab, which likely broke off around or shortly after the time of arc cessation, at ∼165 Ma. Subducting slabs may be dragged horizontally through the mantle over 1,000 km or more, driven by absolute plate motion of the subducting plate (Parsons et al., 2021; Qayyum et al., 2022; Spakman et al., 2018; van de Lagemaat et al., 2018), which implies that the present-day position of the slab remains of the Bonanza arc subduction zone may no longer reflect the location at which subduction started. However, tomography-plate reconstruction correlations suggest that slabs undergo no major horizontal motion after their break-off (Domeier et al., 2016; van der Meer et al., 2010, 2018), which suggests that the Bonanza arc-related slab is likely located in the lower mantle beneath the location where it broke off. This slab is likely one of the western belt slabs that have been identified below and west of NAM (Clennett et al., 2020; Sigloch & Mihalynuk, 2013, 2017; van der Meer et al., 2010, 2012). The southernmost of these, the Malpelo slab west of Colombia, was previously considered a candidate to be linked to the Bonanza arc (van der Meer et al., 2018). However, because the Caribbean and western South American Jurassic to Lower Cretaceous arcs have been located at that paleolatitude (Boschman et al., 2019), these arcs may provide a better candidate to explain the Malpelo slab. The southernmost slab of the western belt that cannot be explained by Caribbean arcs is the Socorro slab (van der Meer et al., 2010, 2018), at a latitude of ∼17°N (Figure 1). It is also not likely that this slab correlates to subduction records of the Guerrero terrane (in Mexico), which was built since Triassic time on accretionary prism rocks formed at the North American margin and was only temporarily separated from NAM by a short-lived and likely narrow back-arc basin (Boschman, Garza, et al., 2018; Boschman, van Hinsbergen, et al., 2018; Busby et al., 2023; Martini et al., 2014). Because the Bonanza arc is the southernmost intra-oceanic arc complex in the Cordilleran orogen, we therefore discuss in our scenarios S and N whether the Socorro slab may have been linked to the Bonanza arc.

Both scenarios share the post-80 Ma history in which paleomagnetic data place the Wrangellia superterrane about 20° south of its present latitude. The declination data are scattered and permit a rotated or a non-rotated position relative to today (Figure 7). In our schematic reconstructions, we place the Wrangellia superterrane in a non-rotated position, parallel to and close to the North American margin. We are well aware of the controversy around this reconstruction (e.g., Johnston, 2008; Trop & Ridgway, 2007), or even around the timing of the Wrangellia superterrane accretion (e.g., Gehrels et al., 2009; Hampton et al., 2010; McClelland et al., 1992; Monger, 2014; Nokleberg et al., 2000; Saleeby, 2000; Stevens Goddard et al., 2018; Tikoff et al., 2023; Trop et al., 2002), or diachroneity of accretion (e.g., Manselle et al., 2020; Nokleberg et al., 2000; Pavlis et al., 2019; Trop & Ridgway, 2007). At this stage, we have no satisfactory solution for where the inferred northward motion, which remains unaccounted for in the structural record, was accommodated. The position of the Wrangellia superterrane in our simple reconstruction is based on paleolatitude data only, and the general agreement that by 80 Ma, the Wrangellia superterrane was located along the North American margin. However, the ∼190–80 Ma history discussed below, during which the northern or southern hemisphere options play a role, would not change if we assumed a more northerly position for the Wrangellia superterrane at 80 Ma.

Scenario N requires ∼5,000 km of northward motion of the Wrangellia superterrane relative to the mantle in the Late Triassic–Early Jurassic, which with southward subduction requires roll-back of the slab below the Bonanza arc. Between 190 and 80 Ma, the Wrangellia superterrane remained at middle latitudes until its collision with NAM, in which case the Bonanza arc was not associated with subduction of the Socorro slab. Another southward dipping subduction zone must therefore have existed between the Wrangellia superterrane and the Farallon Plate, which in Late Jurassic to Early Cretaceous time must have experienced a northward motion component (Arkula et al., 2023; Courtillot et al., 1985; Tarduno et al., 1985, 1986). Reconstructing the Wrangellia superterrane farther south around the mid-Jurassic, as depicted in Figure 8, would require slab advance of the Bonanza subduction zone, combined with another southward dipping subduction zone to accommodate the convergence between the Wrangellia superterrane and the Caribbean lithosphere that remained around equatorial latitudes (Boschman et al., 2019). Finally, the arrival of the Wrangellia superterrane at the North American margin must have involved a complex, counterclockwise plate rotation so that the western margin of the Wrangellia superterrane faced the Panthalassa Ocean. This counterclockwise rotation cannot be reconstructed without generating Farallon-Wrangellia convergence, requiring a syn-rotation, westward dipping subduction zone between these plates.

Scenario S also requires roll-back of the subduction zone below the Wrangellia superterrane in the Late Triassic–Earliest Jurassic, but southward, over ∼15° latitude. This roll-back must have been followed by a northward displacement over as much as 30° until the Middle Jurassic, by which time Caribbean lithosphere was forming to the south of the Wrangellia superterrane around the equator (Boschman et al., 2019). This northward Wrangellia motion occurred during activity of the Bonanza arc, and thus took place during subduction. Hence, it must have been associated with slab advance and dragging over large distances. In Scenario S, it is possible that the Socorro slab represents the lithosphere that detached below the Bonanza arc upon its cessation in the Middle Jurassic. Following this cessation, northward motion of the Wrangellia superterrane continued while the plate carrying it rotated clockwise. This rotation is faster than that reconstructed for the Farallon Plate from Pacific anomalies (e.g., Seton et al., 2012), so it requires that the Wrangellia superterrane was part of a separate plate. However, no subduction zones are required between the Wrangellia superterrane and the Farallon Plate: its clockwise rotation could have been accommodated by subduction between the Wrangellia superterrane and NAM. The systematic northward motions are consistent with the paleomagnetic evidence from accreted OPS (Courtillot et al., 1985; Tarduno et al., 1985, 1986) and North American upper plate ophiolites (Arkula et al., 2023). Subduction reactivation west of the Wrangellia superterrane is only required upon its accretion to NAM (and may thus serve as a constraint on collision age).

7. Conclusions

The Wrangellia superterrane is widely thought to have been part of plate(s) of the eastern Panthalassa Ocean that moved independently and converged (obliquely) with NAM during most of the Mesozoic. In this study, we re-evaluate Wrangellia's paleomagnetic record and conclude with the following key points:

1. Our new paleomagnetic data from Upper Triassic limestones and Lower Jurassic volcanic flows of northern Vancouver Island indicate that the Bonanza arc was located either ∼25–30° North and rotated ∼80° counterclockwise (relative to present-day spin axis), or that it was located ∼25–30° South and rotated ∼100° clockwise.
2. New and previous Triassic to Early Jurassic paleomagnetic data of the Wrangellia superterrane are coherent in terms of inclination and declination throughout a 2,000 km-long stretch of the superterrane that lies south of the Alaskan orocline. This consistency suggests that local vertical-axis rotations linked to post-accretionary tectonics have not obscured the pre-accretionary motions of the Wrangellia superterrane.
3. To consider the hemispheric ambiguity of the paleomagnetic data, we present two scenarios in which the Wrangellia superterrane was located either in the southern hemisphere (Scenario S) or in the northern hemisphere (Scenario N) at ∼190 Ma. From ∼190 to 80 Ma, the Wrangellia superterrane either moved northward while rotating 110° clockwise relative to NAM at a north-dipping subduction zone (Scenario S) or remained at northern middle latitudes while rotating 70° counterclockwise at a south-dipping subduction zone (Scenario N). In both scenarios N and S, the accretion of the Wrangellia superterrane to the Intermontane superterrane must have taken place >1,500 km south of their present location.
4. The main conclusion that can be drawn from comparing these scenarios is that scenario S represents the simplest solution to transport the Wrangellia superterrane from the equator to a position alongside NAM allowing its accretion after a significant (clockwise) rotation. Moreover, Scenario S makes it possible that the

Socorro slab (17° N) represents the lithosphere that detached below the Bonanza arc upon its cessation in the Middle Jurassic. The ∼5,000 km-translation in ∼110 Ma from the southern hemisphere toward NAM is compatible with rates and directions of Jurassic oblique subduction beneath California and Cretaceous OPS motions. In contrast, scenario N requires at least two additional steps in the overall motion of the Wrangellia superterrane toward NAM: (a) after a rapid northward shift of ∼50° in the Late Triassic to Earliest Jurassic, the superterrane moved southward relative to NAM during the Early Jurassic; (b) the superterrane rotated away from NAM during the Middle Jurassic before moving eastward to be accreted to NAM. We prefer the southern hemisphere scenario, but stress that a detailed plate kinematic restoration based on systematic analysis of Cordilleran orogenic architecture is required to fully unveil the implications of both scenarios. In addition, new paleomagnetic investigations of preserved rock records that span the current "data gap" from the Middle Jurassic to mid-Cretaceous are highly needed for improving reconstructions of the pre-accretion history of the Wrangellia superterrane.

Data Availability Statement

New paleomagnetic data can be imported into the Paleomagnetism.org 2.4.0 portal from data files (.col) available in Data Sets S1 and S2, and can also be found in the Paleomagnetism.org database (Andjić et al., 2024, https://paleomagnetism.org/publication?0450afe68406c017af37b4dc8087c7bb601f2e03f8c14b9fcd64a8c4846f5963).

References

Alberts, D., Gehrels, G. E., & Nelson, J. (2021). U-Pb and Hf analyses of detrital zircons from Paleozoic and Cretaceous strata on Vancouver Island, British Columbia: Constraints on the Paleozoic tectonic evolution of southern Wrangellia. *Lithosphere*, *2021*(1), 7866944. https://doi.org/10.2113/2021/7866944

Alvarez, W., Kent, D. V., Premoli Silva, I., Schweikert, R. A., & Larson, R. A. (1980). Franciscan Complex limestone deposited at 17° south paleolatitude. *Geological Society of America Bulletin*, *91*(8), 476–484. https://doi.org/10.1130/0016-7606(1980)91<476:FCLDAS>2.0.CO;2

Amaru, M. L. (2007). Global travel time tomography with 3-D reference models. *Geologica Ultraiectina*, *274*, 174.

Amato, J. M., Pavlis, T. L., Clift, P. D., Kochelek, E. J., Hecker, J. P., Worthman, C. M., & Day, E. M. (2013). Architecture of the Chugach accretionary complex as revealed by detrital zircon ages and lithologic variations: Evidence for Mesozoic subduction erosion in south-central Alaska. *Geological Society of America Bulletin*, *125*(11–12), 1891–1911. https://doi.org/10.1130/B30818.1

Amato, J. M., Rioux, M. E., Kelemen, P. B., Gehrels, G. E., Clift, P. D., Pavlis, T. L., & Draut, A. E. (2007). U-Pb geochronology of volcanic rocks from the Jurassic Talkeetna Formation and detrital zircons from prearc and postarc sequences: Implications for the age of magmatism and inheritance in the Talkeetna arc. *Geological Society of America Special Paper*, *431*, 253–271. https://doi.org/10.1130/2007.2431(11)

Andjić, G., Escuder-Viruete, J., Baumgartner-Mora, C., Baumgartner, P. O., Mitchell, S. F., Caron, M., & Caus, E. (2019). Sedimentary record of arc-continent collision along Mesozoic SW North America (Siuna Belt, Nicaragua). *Tectonics*, *38*(12), 4399–4425. https://doi.org/10.1029/2019TC005741

Andjić, G., Vaes, B., van de Lagemaat, S. H. A., Boschman, L. M., Dekkers, M. J., Johnston, S. T., & van Hinsbergen, D. J. J. (2024). Paleolatitudinal drift and major rotation of the Wrangellia superterrane in the Mesozoic: A signal of east-Panthalassa plate motion? [Dataset]. *Paleomagnetism.org*. https://paleomagnetism.org/publication?0450afe68406c017af37b4dc8087c7bb601f2e03f8c14b9fcd64a8c4846f5963

Arason, Þ., & Levi, S. (2010). Maximum likelihood solution for inclination-only data in paleomagnetism. *Geophysical Journal International*, *182*(2), 753–771. https://doi.org/10.1111/j.1365-246X.2010.04671.x

Arkula, C., Lom, N., Wakabayashi, J., Rea-Downing, G., Qayyum, A., Dekkers, M. J., et al. (2023). The forearc ophiolites of California formed during trench-parallel spreading: Kinematic reconstruction of the western USA Cordillera since the Jurassic. *Earth-Science Reviews*, *237*, 104275. https://doi.org/10.1016/j.earscirev.2022.104275

Bacon, C. R., Vazquez, J. A., & Wooden, J. L. (2012). Peninsular terrane basement ages recorded by Paleozoic and Paleoproterozoic zircon in gabbro xenoliths and andesite from Redoubt volcano, Alaska. *Geological Society of America Bulletin*, *124*(1–2), 24–34. https://doi.org/10.1130/B30439.1

Bazard, D. R., Butler, R. F., Gehrels, G., & Soja, C. M. (1995). Early Devonian paleomagnetic data from the Lower Devonian Karheen Formation suggest Laurentia-Baltica connection for the Alexander terrane. *Geology*, *23*(8), 707–710. https://doi.org/10.1130/0091-7613(1995)023<0707:EDPDFT>2.3.CO;2

Beck, M. E. (1976). Discordant paleomagnetic pole positions as evidence of regional shear in the western Cordillera of North America. *American Journal of Science*, *276*(6), 694–712. https://doi.org/10.2475/ajs.276.6.694

Beck, M. E. (1980). Paleomagnetic record of plate-margin tectonic processes along the western edge of North America. *Journal of Geophysical Research*, *85*(B12), 7115–7131. https://doi.org/10.1029/JB085iB12p07115

Beck, M. E., & Noson, L. (1972). Anomalous paleolatitudes in Cretaceous granitic rocks. *Nature Physical Science*, *235*(53), 11–13. https://doi.org/10.1038/physci235011a0

Beranek, L. P., van Staal, C. R., Gordee, S. M., McClelland, W. C., Israel, S., & Mihalynuk, M. G. (2012). Tectonic significance of Upper Cambrian–Middle Ordovician mafic volcanic rocks on the Alexander terrane, Saint Elias Mountains, northwestern Canada. *The Journal of Geology*, *120*(3), 293–314. https://doi.org/10.1086/664788

Beranek, L. P., van Staal, C. R., McClelland, W. C., Joyce, N., & Israel, S. (2014). Late Paleozoic assembly of the Alexander-Wrangellia-Peninsular composite terrane, Canadian and Alaska Cordillera. *Geological Society of America Bulletin*, *126*, 1531–1550. https://doi.org/10.1130/B31066.1

Bogue, S. W., & Grommé, C. S. (2004). Structural correction of paleomagnetic vectors dispersed about two fold axes and application to the Duke Island (Alaska) ultramafic complex. *Journal of Geophysical Research*, *109*(B11). https://doi.org/10.1029/2004JB002989

Boivin, M.-P., Matthews, W., Coutts, D., & Hubbard, S. (2022). Improved provenance constraints for Nanaimo Group sediments, British Columbia, Canada, through zircon LA-ICP-MS depth-profiling. *Tectonics*, *41*(12), e2021TC007106. https://doi.org/10.1029/2021TC007106

Boschman, L. M., Garza, R. S. M., Langereis, C. G., & van Hinsbergen, D. J. J. (2018). Paleomagnetic constraints on the kinematic relationship between the Guerrero terrane (Mexico) and North America since Early Cretaceous time. *Geological Society of America Bulletin*, *130*(7–8), 1131–1142. https://doi.org/10.1130/B31916.1

Boschman, L. M., van der Wiel, E., Flores, K. E., Langereis, C. G., & van Hinsbergen, D. J. J. (2019). The Caribbean and Farallon plates connected: Constraints from stratigraphy and paleomagnetism of the Nicoya Peninsula, Costa Rica. *Journal of Geophysical Research: Solid Earth*, *124*(7), 6243–6266. https://doi.org/10.1029/2018JB016369

Boschman, L. M., & van Hinsbergen, D. J. J. (2016). On the enigmatic birth of the Pacific Plate within the Panthalassa Ocean. *Science Advances*, *2*(7), e1600022. https://doi.org/10.1126/sciadv.1600022

Boschman, L. M., van Hinsbergen, D. J. J., Kimbrough, D. L., Langereis, C. G., & Spakman, W. (2018). The dynamic history of 220 million years of subduction below Mexico: A correlation between slab geometry and overriding plate deformation based on geology, paleomagnetism, and seismic tomography. *Geochemistry, Geophysics, Geosystems*, *19*(12), 4649–4672. https://doi.org/10.1029/2018GC007739

Boschman, L. M., van Hinsbergen, D. J. J., Langereis, C. G., Flores, K. E., Kamp, P. J. J., Kimbrough, D. L., et al. (2021). Reconstructing lost plates and plate boundaries of the Panthalassa Ocean from circum-Pacific accretionary orogens. *American Journal of Science*, *321*(6), 907–954. https://doi.org/10.2475/06.2021.08

Box, S. E. (1985). Early Cretaceous orogenic belt in northwestern Alaska: Internal organization, lateral extent and tectonic interpretation. In D. G. Howell (Ed.), *Tectonostratigraphic Terranes of the Circum-Pacific Region, Circum-Pacific Council for Energy and Mineral Resources, Earth Science Series* (Vol. 1, pp. 137–145).

Busby, C. J., Morris, R. A., DeBari, S. M., Medynski, S., Putirka, K., Graham, D. M. A., et al. (2023). Geology of a large intact extensional oceanic arc crustal section with superior exposures: Cretaceous Alisitos Arc, Baja California (Mexico). *Geological Society of America Special Paper*, *560*, 1–107. https://doi.org/10.1130/2023.2560(01)

Butler, R. F., Gehrels, G. E., Baldwin, S., & Davidson, C. (2002). Paleomagnetism and geochronology of the Ecstall pluton in the Coast Mountains of British Columbia: Evidence for local deformation rather than large-scale transport. *Journal of Geophysical Research*, *107*(B1), EPM 3-1–EPM 3-13. https://doi.org/10.1029/2001JB000270

Butler, R. F., Gehrels, G. E., & Bazard, D. R. (1997). Paleomagnetism of Paleozoic strata of the Alexander terrane, southeastern Alaska. *Geological Society of America Bulletin*, *109*(10), 1372–1388. https://doi.org/10.1130/0016-7606(1997)109<1372:POPSOT>2.3.CO;2

Butler, R. F., Gehrels, G. E., & Kodama, K. P. (2001). A moderate translation alternative to the Baja British Columbia hypothesis. *GSA Today*, *11*(6), 4–10. https://doi.org/10.1130/1052-5173(2001)011<0004:amtatt>2.0.co;2

Butler, R. F., Gehrels, G. E., & Saleeby, J. B. (2001). Paleomagnetism of the Duke Island, Alaska, ultramafic complex revisited. *Journal of Geophysical Research*, *106*(B9), 19259–19269. https://doi.org/10.1029/2001JB000531

Canil, D., Johnston, S. T., Larocque, J., Friedman, R., & Heaman, L. M. (2013). Age, construction, and exhumation of the midcrust of the Jurassic Bonanza arc, Vancouver Island, Canada. *Lithosphere*, *5*(1), 82–91. https://doi.org/10.1130/L225.1

Canil, D., Styan, J., Larocque, J., Bonnet, E., & Kyba, J. (2010). Thickness and composition of the Bonanza arc crustal section, Vancouver Island, Canada. *Geological Society of America Bulletin*, *122*(7–8), 1094–1105. https://doi.org/10.1130/B26578.1

Caruthers, A. H., Marroquín, S. M., Gröcke, D. R., Golding, M. L., Aberhan, M., Them, T. R., et al. (2022). New evidence for a long Rhaetian from a Panthalassan succession (Wrangell Mountains, Alaska) and regional differences in carbon cycle perturbations at the Triassic-Jurassic transition. *Earth and Planetary Science Letters*, *577*, 117262. https://doi.org/10.1016/j.epsl.2021.117262

Clennett, E. J., Sigloch, K., Mihalynuk, M. G., Seton, M., Henderson, M. A., Hosseini, K., et al. (2020). A quantitative tomotectonic plate reconstruction of western North America and the eastern Pacific basin. *Geochemistry, Geophysics, Geosystems*, *20*(8), e2020GC009117. https://doi.org/10.1029/2020GC009117

Clift, P. D., Draut, A. E., Kelemen, P. B., Blusztajn, J., & Greene, A. (2005). Stratigraphic and geochemical evolution of an oceanic arc upper crustal section: The Jurassic Talkeetna Volcanic Formation, south-central Alaska. *Geological Society of America Bulletin*, *117*(7), 902–925. https://doi.org/10.1130/B25638.1

Clift, P. D., Pavlis, T., DeBari, S. M., Draut, A. E., Rioux, M., & Kelemen, P. K. (2005). Subduction erosion of the Jurassic Talkeetna-Bonanza arc and the Mesozoic accretionary tectonics of western North America. *Geology*, *33*(11), 881–884. https://doi.org/10.1130/G21822.1

Colpron, M., & Nelson, J. L. (2009). A Palaeozoic Northwest Passage: Incursion of Caledonian, Baltican and Siberian terranes into eastern Panthalassa, and the early evolution of the North American Cordillera. *The Geological Society, London, Special Publications*, *318*(1), 273–307. https://doi.org/10.1144/SP318.10

Courtillot, V., Feiberg, H., Ragaru, J. P., Kerguelen, R., McWilliams, M., & Cox, A. (1985). Franciscan Complex limestone deposited at 24°N. *Geology*, *13*(2), 107–110. https://doi.org/10.1130/0091-7613(1985)13<107:FCLDAN>2.0.CO;2

Cowan, D. S., Brandon, M., & Garver, J. I. (1997). Geologic tests of hypotheses for large coastwise displacements–a critique illustrated by the Baja British Columbia controversy. *American Journal of Science*, *297*, 117–133. https://doi.org/10.2475/ajs.297.2.117

Dal Corso, J., Bernardi, M., Sun, Y., Song, H., Seyfullah, L. J., Preto, N., et al. (2020). Extinction and dawn of the modern world in the Carnian (Late Triassic). *Science Advances*, *6*(38), eaba0099. https://doi.org/10.1126/sciadv.aba00

DeBari, S., Anderson, R. G., & Mortensen, J. K. (1999). Correlation among lower to upper crustal components in an island arc: The Jurassic Bonanza arc, Vancouver Island. Canada. *Canadian Journal of Earth Sciences*, *36*(8), 1371–1413. https://doi.org/10.1139/e99-029

Deenen, M. H. L., Langereis, C. G., van Hinsbergen, D. J. J., & Biggin, A. J. (2011). Geomagnetic secular variation and the statistics of palaeomagnetic directions. *Geophysical Journal International*, *186*(2), 509–520. https://doi.org/10.1111/j.1365-246X.2011.05050.x

Dickinson, W. R. (2004). Evolution of the North American Cordillera. *Annual Review of Earth and Planetary Sciences*, *32*(1), 13–45. https://doi.org/10.1146/annurev.earth.32.101802.120257

Dickinson, W. R., & Butler, R. F. (1998). Coastal and Baja California paleomagnetism reconsidered. *Geological Society of America Bulletin*, *110*(10), 1268–1280. https://doi.org/10.1130/0016-7606(1998)110<1268:CABCPR>2.3.CO;2

Domeier, M., Doubrovine, P. V., Torsvik, T. H., Spakman, W., & Bull, A. L. (2016). Global correlation of lower mantle structure and past subduction. *Geophysical Research Letters*, *43*(10), 4945–4953. https://doi.org/10.1002/2016GL068827

Dover, J. H. (1994). Geology of part of east-central Alaska. In G. Plafker & H. C. Berg (Eds.), *The geology of Alaska, GSA Decade of North American Geology* (Vol. G–1, pp. 153–204). https://doi.org/10.1130/DNAG-GNA-G1.153

D'Souza, R. J., Canil, D., & Creaser, R. A. (2016). Assimilation, differentiation, and thickening during formation of arc crust in space and time: The Jurassic Bonanza arc, Vancouver Island, Canada. *Geological Society of America Bulletin*, *128*(3–4), 543–557. https://doi.org/10.1130/B31289.1

Engebretson, D. C., Cox, A., & Gordon, R. G. (1985). Relative motions between oceanic and continental plates in the Pacific Basin. *Geological Society of America Special Paper*, *206*, 59–60. https://doi.org/10.1130/SPE206-p1

Enkin, R. J. (2006). Paleomagnetism and the case for Baja British Columbia. In J. Haggart, R. J. Enkin, & J. W. H. Monger (Eds.), *Paleogeography of the North American Cordillera: Evidence for and Against Large-Scale Displacements, Geological Association of Canada, Special Paper* (Vol. 46, pp. 233–253).

Enkin, R. J., Baker, J., & Mustard, P. S. (2001). Paleomagnetism of the Upper Cretaceous Nanaimo Group, southwestern Canadian Cordillera. *Canadian Journal of Earth Sciences*, *38*(10), 1403–1422. https://doi.org/10.1139/cjes-38-10-1403

Fisher, R. (1953). Dispersion on a sphere. *Proceedings of the Royal Society of London, Series A, Mathematical and Physical Sciences*, *217*(1130), 295–305. https://doi.org/10.1098/rspa.1953.0064

Fuston, S., & Wu, J. (2021). Raising the Resurrection plate from an unfolded-slab plate tectonic reconstruction of northwestern North America since early Cenozoic time. *Geological Society of America Bulletin*, *133*(5–6), 1128–1140. https://doi.org/10.1130/B35677.1

Gallo, L. C., Domeier, M., Sapienza, F., Swanson-Hysell, N. L., Vaes, B., Zhang, Y., et al. (2023). Embracing uncertainty to resolve polar wander: A case study of Cenozoic North America. *Geophysical Research Letters*, *50*(11), e2023GL103436. https://doi.org/10.1029/2023GL103436

Gehrels, G., Rusmore, M., Woodsworth, G., Crawford, M., Andronicos, C., Hollister, L., et al. (2009). U–Th–Pb geochronology of the Coast Mountains batholith in north-coastal British Columbia: Constraints on age and tectonic evolution. *Geological Society of America Bulletin*, *121*(9–10), 1341–1361. https://doi.org/10.1130/B26404.1

Gehrels, G. E., & Saleeby, J. B. (1987). Geologic framework, tectonic evolution, and displacement history of the Alexander terrane. *Tectonics*, *6*(2), 151–173. https://doi.org/10.1029/TC006i002p00151

Gerritsen, D., Vaes, B., & van Hinsbergen, D. J. J. (2022). Influence of data filters on the position and precision of paleomagnetic poles: What is the optimal sampling strategy? *Geochemistry, Geophysics, Geosystems*, *23*(4), e2021GC010269. https://doi.org/10.1029/2021GC010269

Greene, A. R., Scoates, J. S., Weis, D., Katvala, E. C., Israel, S., & Nixon, G. T. (2010). The architecture of oceanic plateaus revealed by the volcanic stratigraphy of the accreted Wrangellia oceanic plateau. *Geosphere*, *6*(1), 47–73. https://doi.org/10.1130/GES00212.1

Guilmette, C., Smit, M., van Hinsbergen, D. J. J., Gürer, D., Maffione, M., Rabeau, O., et al. (2018). Forced subduction initiation recorded in the sole and crust of the Semail ophiolite of Oman. *Nature Geoscience*, *11*(9), 688–695. https://doi.org/10.1038/s41561-018-0209-2

Haeussler, P. J., Coe, R. S., & Onstott, T. C. (1992). Paleomagnetism of the Late Triassic Hound Island Volcanics: Revisited. *Journal of Geophysical Research*, *97*(B13), 19617–19639. https://doi.org/10.1029/92JB01361

Haeussler, P. J., Coe, R. S., & Renne, P. (1992). Paleomagnetism and geochronology of 23 Ma gabbroic intrusions in the Keku Strait, Alaska, and implications for the Alexander terrane. *Journal of Geophysical Research*, *97*(B13), 19641–19651. https://doi.org/10.1029/92JB01360

Hampton, B. A., Ridgway, K. D., & Gehrels, G. E. (2010). A detrital record of Mesozoic island arc accretion and exhumation in the North American Cordillera: U-Pb geochronology of the Kahiltna basin, southern Alaska. *Tectonics*, *29*(4), TC4015. https://doi.org/10.1029/2009tc002544

Harbert, W. (1990). Paleomagnetic data from Alaska: Reliability, interpretation and terrane trajectories. *Tectonophysics*, *184*(1), 111–135. https://doi.org/10.1016/0040-1951(90)90124-Q

Harrison, C. G. A., & Lindh, T. (1982). A polar wandering curve for North America during the Mesozoic and Cenozoic. *Journal of Geophysical Research*, *87*(B3), 1903–1920. https://doi.org/10.1029/JB087iB03p01903

Heslop, D., Scealy, J. L., Wood, A. T. A., Tauxe, L., & Roberts, A. P. (2023). A bootstrap common mean direction test. *Journal of Geophysical Research: Solid Earth*, *128*(8), e2023JB026983. https://doi.org/10.1029/2023JB026983

Hildebrand, R. S. (2013). Mesozoic assembly of the North American Cordillera. *Geological Society of America Special Paper*, *495*, 1–170. https://doi.org/10.1130/SPE495

Hillhouse, J. W. (1977). Paleomagnetism of the Triassic Nikolai Greenstone, south-central Alaska. *Canadian Journal of Earth Sciences*, *14*(11), 2578–2592. https://doi.org/10.1139/e77-223

Hillhouse, J. W. (1987). Accretion of southern Alaska. *Tectonophysics*, *139*(1–2), 107–122. https://doi.org/10.1016/0040-1951(87)90200-9

Hillhouse, J. W., & Grommé, C. S. (1980). Paleomagnetism of the Triassic Hound Island Volcanics, Alexander Terrane, southeastern Alaska. *Journal of Geophysical Research*, *85*(B5), 2594–2602. https://doi.org/10.1029/JB085iB05p02594

Hillhouse, J. W., & Grommé, C. S. (1984). Northward displacement and accretion of Wrangellia: New paleomagnetic evidence from Alaska. *Journal of Geophysical Research*, *89*(B6), 4461–4477. https://doi.org/10.1029/JB089iB06p04461

Hillhouse, J. W., Grommé, C. S., & Csejtey, B. (1985). Tectonic implications of paleomagnetic poles from Lower Tertiary Volcanic Rocks, south central Alaska. *Journal of Geophysical Research*, *90*(B14), 12523–12535. https://doi.org/10.1029/JB090iB14p12523

Hollister, L. S., Hargraves, R. B., James, T. S., & Renne, P. R. (2004). The paleomagnetic effects of reheating of the Ecstall pluton, British Columbia. *Earth and Planetary Science Letters*, *221*(1–4), 397–407. https://doi.org/10.1016/S0012-821X(04)00067-6

Housen, B. A. (2018). Paleomagnetism and rotation history of the Blue Mountains, Oregon, USA. In R. V. Ingersoll, T. F. Lawton, & S. A. Graham (Eds.), *Tectonics, sedimentary basins, and provenance: A Celebration of William R. Dickinson's Career, Geological Society of America Special Paper* (Vol. 540, pp. 223–233). https://doi.org/10.1130/2018.2540(10)

Housen, B. A., & Beck, M. E. (1999). Testing terrane transport: An inclusive approach to the Baja B.C. controversy. *Geology*, *27*(12), 1143–1146. https://doi.org/10.1130/0091-7613(1999)027<1143:tttaia>2.3.co;2

Hults, C. P., Wilson, F. H., Donelick, R. A., & O'Sullivan, P. B. (2013). Two flysch belts having distinctly different provenance suggest no stratigraphic link between the Wrangellia composite terrane and the paleo-Alaskan margin. *Lithosphere*, *5*(6), 575–594. https://doi.org/10.1130/L310.1

Irving, E., & Brandon, M. T. (1990). Paleomagnetism of the Flores volcanics, Vancouver Island, in place by Eocene time. *Canadian Journal of Earth Sciences*, *27*(6), 811–817. https://doi.org/10.1139/e90-083

Irving, E., & Massey, N. W. D. (1990). Paleomagnetism of ocean layers 2 and 3: Evidence from the Metchosin Complex, Vancouver Island. *Physics of the Earth and Planetary Interiors*, *64*(2–4), 247–260. https://doi.org/10.1016/0031-9201(90)90041-U

Irving, E., Woodsworth, G. J., Wynne, P. J., & Morrison, A. (1985). Paleomagnetic evidence for displacement from the south of the Coast Plutonic Complex, British Columbia. *Canadian Journal of Earth Sciences*, *22*(4), 584–598. https://doi.org/10.1139/e85-058

Irving, E., & Wynne, P. J. (1990). Palaeomagnetic evidence bearing on the evolution of the Canadian Cordillera. *Philosophical Transactions of the Royal Society of London. Series A, Mathematical and Physical Sciences*, *331*(1620), 487–509.

Irving, E., Wynne, P. J., Thorkelson, D. J., & Schiarizza, P. (1996). Large (1000–4000 km) northward movements of tectonic domains in the northern Cordillera, 83 to 45 Ma. *Journal of Geophysical Research*, *101*(B8), 17901–17916. https://doi.org/10.1029/96JB01181

Irving, E., & Yole, R. W. (1987). Tectonic rotations and translations in Western Canada—New evidence from Jurassic rocks of Vancouver Island. *Geophysical Journal of the Royal Astronomical Society*, *91*(3), 1025–1048. https://doi.org/10.1111/j.1365-246X.1987.tb01678.x

Isozaki, Y., Maruyama, S., & Furuoka, F. (1990). Accreted oceanic materials in Japan. *Tectonophysics*, *181*(1–4), 179–205. https://doi.org/10.1016/0040-1951(90)90016-2

Israel, S., Beranek, L. P., Friedman, R. M., & Crowley, J. L. (2014). New ties between the Alexander terrane and Wrangellia and implications for North America Cordilleran evolution. *Lithosphere*, *6*(4), 270–276. https://doi.org/10.1130/L364.1

Johnson, C. L., Constable, C. G., Tauxe, L., Barendregt, R., Brown, L. L., Coe, R. S., et al. (2008). Recent investigations of the 0-5 Ma geomagnetic field recorded by lava flows. *Geochemistry, Geophysics, Geosystems*, *9*(4), Q04032. https://doi.org/10.1029/2007GC001696

Johnston, S. T. (2001). The Great Alaskan Terrane Wreck: Reconciliation of paleomagnetic and geological data in the Northern Cordillera. *Earth and Planetary Science Letters*, *193*(3–4), 259–272. https://doi.org/10.1016/S0012-821X(01)00516-7

Johnston, S. T. (2008). The Cordilleran ribbon continent of North America. *Annual Review of Earth and Planetary Sciences*, *36*(1), 495–530. https://doi.org/10.1146/annurev.earth.36.031207.124331

Journeay, J. M., & Friedman, R. M. (1993). The Coast Belt thrust system: Evidence of Late Cretaceous shortening in southwestern British Columbia. *Tectonics*, *12*, 756–776. https://doi.org/10.1029/92TC02773

Kent, D. V., & Irving, E. (2010). Influence of inclination error in sedimentary rocks on the Triassic and Jurassic apparent pole wander path for North America and implications for Cordilleran tectonics. *Journal of Geophysical Research*, *115*(B10), B10103. https://doi.org/10.1029/2009JB007205

Kim, B., & Kodama, K. P. (2004). A compaction correction for the paleomagnetism of the Nanaimo Group sedimentary rocks: Implications for the Baja British Columbia hypothesis. *Journal of Geophysical Research*, *109*(B2), B02102. https://doi.org/10.1029/2003JB002696

Kirschvink, J. L. (1980). The least-squares line and plane and the analysis of palaeomagnetic data. *Geophysical Journal International*, *62*(3), 699–718. https://doi.org/10.1111/j.1365-246X.1980.tb02601.x

Koymans, M. R., Langereis, C. G., Pastor-Galan, D., & van Hinsbergen, D. J. J. (2016). Paleomagnetism.org: An online multi-platform open source environment for paleomagnetic data analysis. *Computers & Geosciences*, *93*, 127–137. https://doi.org/10.1016/j.cageo.2016.05.007

Koymans, M. R., van Hinsbergen, D. J. J., Pastor-Galan, D., Vaes, B., & Langereis, C. G. (2020). Towards FAIR paleomagnetic data management through Paleomagnetism.org 2.0. *Geochemistry, Geophysics, Geosystems*, *21*(2), e2019GC008838. https://doi.org/10.1029/2019GC008838

Krijgsman, W., & Tauxe, L. (2006). E/I corrected paleolatitudes for the sedimentary rocks of the Baja British Columbia hypothesis. *Earth and Planetary Science Letters*, *242*(1–2), 205–216. https://doi.org/10.1016/j.epsl.2005.11.052

Kuniyoshi, S., & Liou, J. G. (1976). Burial metamorphism of the Karmutsen volcanic rocks, northeastern Vancouver Island, British Columbia. *American Journal of Science*, *276*(9), 1096–1119. https://doi.org/10.2475/ajs.276.9.1096

Lei, J. Z. X., Golding, M. L., & Husson, J. M. (2020). Analyzing spatial patterns of thermal alteration in the Stikine and Wrangell terranes of the Canadian Cordillera using the conodont color alteration index (CAI) to identify hot spots and cold spots. *Geological Survey of Canada Open File*, *8746*, 43. https://doi.org/10.4095/327243

Mahoney, J. B., Haggart, J. W., Grove, M., Kimbrough, D. L., Isava, V., Link, P. K., et al. (2021). Evolution of the Late Cretaceous Nanaimo Basin, British Columbia, Canada: Definitive provenance links to northern latitudes. *Geosphere*, *17*(6), 2197–2233. https://doi.org/10.1130/GES02394.1

Mahoney, J. B., Mustard, P. S., Haggart, J. W., Friedman, R. M., Fanning, C. M., Mcnicoll, V. J., & Charlotte, Q. (1999). Archean zircons in Cretaceous strata of the western Canadian Cordillera: The "Baja B.C." hypothesis fails a "crucial test". *Geology*, *27*(3), 195–198. https://doi.org/10.1130/0091-7613(1999)027<0195:azicso>2.3.co;2

Manselle, P., Brueseke, M. E., Trop, J. M., Benowitz, J. A., Snyder, D. C., & Hart, W. K. (2020). Geochemical and stratigraphic analysis of the Chisana Formation, Wrangellia terrane, eastern Alaska: Insights into Early Cretaceous magmatism and tectonics along the northern Cordilleran margin. *Tectonics*, *39*(8), e2020TC006131. https://doi.org/10.1029/2020TC006131

Martini, M., Solari, L., & López-Martínez, M. (2014). Correlating the Arperos Basin from Guanajuato, central Mexico, to Santo Tomás, southern Mexico: Implications for the paleogeography and origin of the Guerrero terrane. *Geosphere*, *10*(6), 1385–1401. https://doi.org/10.1130/GES01055.1

Matthews, W. A., Guest, B., Coutts, D. S., Bain, H., & Hubbard, S. M. (2017). Detrital zircons from the Nanaimo Basin, Vancouver Island, British Columbia: An independent test of Late Cretaceous to Cenozoic northward translation. *Tectonics*, *36*(5), 854–876. https://doi.org/10.1002/2017TC004531

McClelland, W. C., Gehrels, G. E., & Saleeby, J. B. (1992). Upper Jurassic–Lower Cretaceous basinal strata along the Cordilleran margin: Implications for the accretionary history of the Alexander-Wrangellia-Peninsular terrane. *Tectonics*, *11*(4), 823–835. https://doi.org/10.1029/92TC00241

McFadden, P., & McElhinny, M. (1988). The combined analysis of remagnetization circles and direct observations in palaeomagnetism. *Earth and Planetary Science Letters*, *87*(1–2), 161–172. https://doi.org/10.1016/0012-821X(88)90072-6

McLaughlin, R. J., Kling, S. A., Poore, R. Z., McDougall, K., & Beutner, E. C. (1982). Post-middle Miocene Accretion of Franciscan Rocks, Northwestern California. *Geological Society of America Bulletin*, *93*(7), 595–605. https://doi.org/10.1130/0016-7606(1982)93<595:pmaofr>2.0.co;2

Meert, J. G., Pivarunas, A. F., Evans, D. A. D., Pisarevsky, S. A., Pesonen, L. J., Li, Z.-X., et al. (2020). The magnificent seven: A proposal for modest revision of the Van der Voo (1990) quality index. *Tectonophysics*, *790*, 228549. https://doi.org/10.1016/j.tecto.2020.228549

Mirzaei, M., Housen, B. A., Burmester, R. F., & Foreman, B. Z. (2021). Paleomagnetic results from Upper Triassic and Middle Jurassic strata of east-central New Mexico, and implication for North American apparent polar wander path. *Tectonophysics*, *811*, 228872. https://doi.org/10.1016/j.tecto.2021.228872

Monger, J. W. H. (2014). Logan Medallist 1. Seeking the suture: The Coast-Cascade conundrum. *Geoscience Canada*, *41*(4), 1–20. https://doi.org/10.12789/geocanj.2014.41.058

Monger, J. W. H., & Price, R. A. (1996). Comment on "Paleomagnetism of the Upper Cretaceous strata of Mount Tatlow: Evidence for 3000 km of northward displacement of the eastern Coast Belt, British Columbia" by P. J. Wynne et al., and on "Paleomagnetism of the Spences Bridge Group and northward displacement of the Intermontane Belt, British Columbia: A second look" by E. Irving et al. *Journal of Geophysical Research*, *101*(B6), 13793–13799. https://doi.org/10.1029/96JB00795

Monger, J. W. H., Price, R. A., & Tempelman-Kluit, J. D. (1982). Tectonic accretion and the origin of the two major metamorphic and plutonic welts in the Canadian Cordillera. *Geology*, *10*(2), 70–75. https://doi.org/10.1130/0091-7613(1982)10<70:TAATOO>2.0.CO;2

Morris, R., & Canil, D. (2022). CO_2 transport at shallow depths in arc magmas: Evidence from unique orbicular dikes in the Jurassic Bonanza arc, Vancouver Island, Canada. *Contributions to Mineralogy and Petrology*, *177*, 6. https://doi.org/10.1007/s00410-021-01852-y

Mulcahy, S. R., Starnes, J. K., Day, H. W., Coble, M. A., & Vervoort, J. D. (2018). Early onset of Franciscan subduction. *Tectonics*, *37*(5), 1194–1209. https://doi.org/10.1029/2017TC004753

Mullender, T. A., Frederichs, T., Hilgenfeldt, C., de Groot, L. V., Fabian, K., & Dekkers, M. J. (2016). Automated paleomagnetic and rock magnetic data acquisition with an in-line horizontal "2G" system. *Geochemistry, Geophysics, Geosystems*, *17*(9), 3546–3559. https://doi.org/10.1002/2016GC006436

Mullender, T. A. T., van Velzen, A. J., & Dekkers, M. J. (1993). Continuous drift correction and separate identification of ferromagnetic and paramagnetic contributions in thermomagnetic runs. *Geophysical Journal International*, *114*(3), 663–672. https://doi.org/10.1111/j.1365-246X.1993.tb06995.x

Müller, R. D., Flament, N., Cannon, J., Tetley, M. G., Williams, S. E., Cao, X., et al. (2022). A tectonic-rules-based mantle reference frame since 1 billion years ago – Implications for supercontinent cycles and plate–mantle system evolution. *Solid Earth*, *13*(7), 1127–1159. https://doi.org/10.5194/se-13-1127-2022

Muttoni, G., & Kent, D. V. (2019). Jurassic monster polar shift confirmed by sequential paleopoles from Adria, promontory of Africa. *Journal of Geophysical Research: Solid Earth*, *124*(4), 3288–3306. https://doi.org/10.1029/2018JB017199

Nelson, J., & Colpron, M. (2007). Tectonics and metallogeny of the British Columbia, Yukon and Alaskan Cordillera, 1.8 Ga to the present. *Geological Association of Canada Mineral Deposits Division Special Publication*, *5*, 755–791.

Nixon, G. T., Hammack, J. L., Hamilton, J. V., Jennings, H., Larocque, J. P., Orr, A. J., et al. (2011). Geology, Geochronology, Lithogeochemistry and Metamorphism of the Mahatta Creek Area, Northern Vancouver Island. *British Columbia Geological Survey Geoscience Map, 2011-3, 1: 50 000 scale*.

Nixon, G. T., Hammack, J. L., Koyanagi, V. M., Payie, G. J., Orr, A. J., Haggart, J. W., et al. (2011). Geology, Geochronology, Lithogeochemistry and Metamorphism of the Quatsino-Port McNeill Area, Northern Vancouver Island. *British Columbia Geological Survey Geoscience Map, 2011-2, 1:50 000 scale*.

Nixon, G. T., Hammack, J. L., Koyanagi, V. M., Snyder, L. D., Payie, G. J., Panteleyev, A., et al. (2011). Geology, Geochronology, Lithogeochemistry and Metamorphism of the Holberg-Winter Harbour Area, Northern Vancouver Island. *British Columbia Geological Survey Geoscience Map, 2011-1, 1:50 000 scale*.

Nixon, G. T., & Orr, A. J. (2007). Recent revisions to the Early Mesozoic stratigraphy of northern Vancouver Island (NTS 102I; 92L) and metallogenic implications, British Columbia. *British Columbia Ministry of Energy, Mines and Petroleum Resources, Geological Fieldwork 2006, Paper 2007-1, 163–177*.

Nixon, G. T., Snyder, L. D., Payie, G. J., Long, S., Finnie, A., Orr, A. J., et al. (2011). Geology, Geochronology, Lithogeochemistry and Metamorphism of the Alice Lake Area, Northern Vancouver Island. *British Columbia Geological Survey Geoscience Map, 2011-4, 1:50 000 scale*.

Nokleberg, W. J., Bundtzen, T. K., Eremin, R. A., Ratkin, V. V., Dawson, K. M., Shpikerman, V. I., et al. (2005). In *Metallogenesis and Tectonics of the Russian Far East, Alaska and the Canadian Cordillera. United States Geological Survey Professional Paper* (Vol. 1697, p. 397).

Nokleberg, W. J., Parfenov, L. M., Monger, J. W. H., Baranov, B. V., Byalobzhesky, S. G., Bundtzen, T. K., et al. (1994). Circum-North Pacific tectono-stratigraphic terrane map. *United States Geological Survey Open-File Report, 94–714* (p. 210). 4 sheets, scales 1:5,000,000, 1: 10,000,000.

Nokleberg, W. J., Parfenov, L. M., Monger, J. W. H., Norton, I. O., Khanchuk, A. I., Stone, D. B., et al. (2000). Phanerozoic tectonic evolution of the Circum-North Pacific. *United States Geological Survey Professional Paper*, *1626*, 122.

Opdyke, N. D., & Channell, J. E. T. (1996). *Magnetic Stratigraphy* (p. 346). Academic Press.

Panuska, B. C. (1985). Paleomagnetic evidence for a post-Cretaceous accretion of Wrangellia. *Geology*, *13*(12), 880–883. https://doi.org/10.1130/0091-7613(1985)13<880:PEFAPA>2.0.CO;2

Panuska, B. C., Decker, J. E., & Berg, H. C. (1984). A preliminary paleomagnetic study of the Gravina-Nutzotin belt, southern and southeastern Alaska. *United States Geological Survey Circular*, *868*, 117–120.

Panuska, B. C., & Stone, D. B. (1981). Late Paleozoic paleomagnetic data for Wrangellia; resolution of the polarity ambiguity. *Nature*, *293*(5833), 561–563. https://doi.org/10.1038/293561a0

Parsons, A. J., Sigloch, K., & Hosseini, K. (2021). Australian plate subduction is responsible for northward motion of the India-Asia collision zone and ~1,000 km lateral migration of the Indian slab. *Geophysical Research Letters*, *48*(18), e2021GL094904. https://doi.org/10.1029/2021GL094904

Passier, H. F., de Lange, G. J., & Dekkers, M. J. (2001). Rock-magnetic properties and geochemistry of the active oxidation front and the youngest sapropel in the Mediterranean. *Geophysical Journal International*, *145*, 604–614. https://doi.org/10.1046/j.0956-540x.2001.01394.x

Pastor-Galán, D., Dekkers, M. J., Gutiérrez-Alonso, G., Brouwer, D., Groenewegen, T., Krijgsman, W., et al. (2016). Paleomagnetism of the Central Iberian curve's putative hinge: Too many oroclines in the Iberian Variscides. *Gondwana Research*, *39*, 96–113. https://doi.org/10.1016/j.gr.2016.06.016

Pavlis, T. L., Amato, J. M., Trop, J. M., Ridgway, K. D., Roeske, S. M., & Gehrels, G. E. (2019). Subduction polarity in ancient arcs: A call to integrate geology and geophysics to decipher the Mesozoic tectonic history of the northern Cordillera of North America. *GSA Today*, *29*(11), 4–10. https://doi.org/10.1130/GSATG402A.1

Pierce, J., Zhang, Y., Hodgin, E. B., & Swanson-Hysell, N. L. (2022). Quantifying inclination shallowing and representing flattening uncertainty in sedimentary paleomagnetic poles. *Geochemistry, Geophysics, Geosystems*, *23*(11), e2022GC010682. https://doi.org/10.1029/2022GC010682

Plafker, G., & Berg, H. D. (1994). Overview of the geology and tectonic evolution of Alaska. In G. Plafker & H. C. Berg (Eds.), *The geology of Alaska, GSA Decade of North American Geology* (Vol. G–1, pp. 989–1021). https://doi.org/10.1130/DNAG-GNA-G1.989

Plafker, G., Nokleberg, W. J., & Lull, J. S. (1989). Bedrock geology and tectonic evolution of the Wrangellia, Peninsular, and Chugach terranes along the Trans-Alaskan crustal transect in the northern Chugach Mountains and southern Copper River basin, Alaska. *Journal of Geophysical Research*, *94*(B4), 4255–4295. https://doi.org/10.1029/JB094iB04p04255

Qayyum, A., Lom, N., Advokaat, E. L., Spakman, W., van der Meer, D. G., & van Hinsbergen, D. J. J. (2022). Subduction and slab detachment under moving trenches during ongoing India-Asia convergence. *Geochemistry, Geophysics, Geosystems*, *23*(11), e2022GC010336. https://doi.org/10.1029/2022GC010336

Rioux, M., Hacker, B., Mattinson, J., Kelemen, P., Blusztajn, J., & Gehrels, G. (2007). Magmatic development of an intra-oceanic arc: High-precision U-Pb zircon and whole-rock isotopic analyses from the accreted Talkeetna arc, south-central Alaska. *Geological Society of America Bulletin*, *119*(9–10), 1168–1184. https://doi.org/10.1130/B25964.1

Rioux, M., Mattinson, J., Hacker, B., Kelemen, P., Blusztajn, J., Hanghøj, K., & Gehrels, G. (2010). Intermediate to felsic middle crust in the accreted Talkeetna arc, the Alaska Peninsula and Kodiak Island, Alaska: An analogue for low-velocity middle crust in modern arcs. *Tectonics*, *29*(3), TC3001. https://doi.org/10.1029/2009TC002541

Roeske, S. M., Mattinson, J. M., & Armstrong, R. L. (1989). Isotopic ages of glaucophane schists on the Kodiak Islands, southern Alaska, and their implications for the Mesozoic tectonic history of the Border Ranges fault system. *Geological Society of America Bulletin*, *101*(8), 1021–1037. https://doi.org/10.1130/0016-7606(1989)101<1021:IAOGSO>2.3.CO;2

Rowley, D. B. (2019). Comparing paleomagnetic study means with apparent wander paths: A case study and paleomagnetic test of the Greater India versus Greater Indian Basin hypotheses. *Tectonics*, *38*(2), 722–740. https://doi.org/10.1029/2017TC004802

Rusmore, M. E., Bogue, S. W., & Woodsworth, G. J. (2013). Paleogeography of the Insular and Intermontane terranes reconsidered: Evidence from the southern Coast Mountains Batholith, British Columbia. *Lithosphere*, *5*, 521–536. https://doi.org/10.1130/10.1130/L288.1

van der Meer, D. G., Torsvik, T. H., Spakman, W., van Hinsbergen, D. J. J., & Amaru, M. L. (2012). Intra-Panthalassa Ocean subduction zones revealed by fossil arcs and mantle structure. *Nature Geoscience*, *5*(3), 215–219. https://doi.org/10.1038/ngeo1401

van der Meer, D. G., van Hinsbergen, D. J. J., & Spakman, W. (2018). Atlas of the Underworld: Slab remnants in the mantle, their sinking history, and a new outlook on lower mantle viscosity. *Tectonophysics*, *723*, 309–448. https://doi.org/10.1016/j.tecto.2017.10.004

Van der Voo, R., Jones, M., Grommé, C. S., Eberlein, G. D., & Churkin, M. (1980). Paleozoic paleomagnetism and northward drift of the Alexander Terrane, southeastern Alaska. *Journal of Geophysical Research*, *85*(B10), 5281–5296. https://doi.org/10.1029/JB085iB10p05281

van Hinsbergen, D. J. J., de Groot, L. V., van Schaik, S. J., Spakman, W., Bijl, P. K., Sluijs, A., et al. (2015). A paleolatitude calculator for paleoclimate studies. *PLoS One*, *10*(6), e0126946. https://doi.org/10.1371/journal.pone.0126946

van Velzen, A. J., & Zijderveld, J. (1995). Effects of weathering on single-domain magnetite in Early Pliocene marine marls. *Geophysical Journal International*, *121*(1), 267–278. https://doi.org/10.1111/j.1365-246X.1995.tb03526.x

Wakabayashi, J. (2015). Anatomy of a subduction complex: Architecture of the franciscan complex, California, at multiple length and time scales. *International Geology Review*, *57*(5–8), 669–746. https://doi.org/10.1080/00206814.2014.998728

Ward, P. D., Hurtado, J. M., Kirschvink, J. L., & Verosub, K. L. (1997). Measurements of the Cretaceous Paleolatitude of Vancouver Island: Consistent with the Baja–British Columbia hypothesis. *Science*, *277*(5332), 1642–1645. https://doi.org/10.1126/science.277.5332.16

White, C., Gehrels, G. E., Pecha, M., Giesler, D., Yokelson, I., McClelland, W. C., & Butler, R. F. (2016). U-Pb and Hf isotope analysis of detrital zircons from Paleozoic strata of the southern Alexander terrane (Southeast Alaska). *Lithosphere*, *8*(1), 83–96. https://doi.org/10.1130/L475.1

Yokelson, I., Gehrels, G. E., Pecha, M., Giesler, D., White, C., & McClelland, W. C. (2015). U-Pb and Hf isotope analysis of detrital zircons from Mesozoic strata of the Gravina belt, southeast Alaska. *Tectonics*, *34*(10), 2052–2066. https://doi.org/10.1002/2015TC003955

Yole, R. W., & Irving, E. (1980). Displacement of Vancouver Island: Paleomagnetic evidence from the Karmutsen Formation. *Canadian Journal of Earth Sciences*, *17*(9), 1210–1228. https://doi.org/10.1139/e80-127

Zijderveld, J. D. A. (1967). A.C. Demagnetization of rocks: Analysis of results. *Developments in Solid Earth Geophysics*, *3*, 254–286. https://doi.org/10.1016/B978-1-4832-2894-5.50049-5